Snappability and singularity-distance of pin-jointed body-bar frameworks

Georg Nawratil

Institute of Discrete Mathematics and Geometry & Center for Geometry and Computational Design
TU Wien
Wiedner Hauptstrasse 8-10/104, Vienna 1040, Austria
Email: nawratil@geometrie.tuwien.ac.at

ABSTRACT

It is well-known that there exist rigid frameworks whose physical models can snap between different realizations due to non-destructive elastic deformations of material. We present a method to measure this snapping capability based on the total elastic strain energy density of the framework by using the physical concept of Green-Lagrange strain. As this so-called snappability only depends on the intrinsic framework geometry, it enables a fair comparison of pin-jointed body-bar frameworks, thus it can serve engineers as a criterion within the design process of multistable mechanisms. Moreover, it turns out that the value obtained from this intrinsic pseudometric also gives the distance to the closest shaky configuration in the case of isostatic frameworks. Therefore it is suited for the computation of these singularity-distances for diverse mechanical devices. In more detail we study this problem for parallel manipulators of Stewart-Gough type.

1 Introduction

In this paper we study frameworks composed of bars and bodies linked by pin-joints, which are rotational joints in the planar case and spherical joints in the spatial case. Note that all joints are assumed to be without clearance. A body is either a polyhedron or a polygonal panel[1]. For both of these cases it is assumed that the body does not possess any unnecessary vertices; i.e. each of its vertices is pin-jointed. An additional assumption is that the inner graph of each body is globally rigid, where an inner graph is defined as follows:

Definition 1. *Connect all vertices of the polyhedron (polygonal panel) by edges, which are either located on the boundary of the polyhedron (polygon) or in its interior. The resulting graph is called inner graph.*

Note that our studied class of geometric structures known as *pin-jointed body-bar frameworks* also contains hinge-jointed frameworks, as a hinge between two bodies can be replaced by two pin-joints.

By defining the combinatorial structure of the framework as well as the lengths of the bars and the shapes of the bodies, respectively, the intrinsic geometry of the framework is fixed. In general the assignment of the intrinsic metric does not uniquely determine the embedding of the framework into the Euclidean space, thus such a framework can have different incongruent realizations.

A realization is called a snapping realization if it is *close enough* to another incongruent realization such that the physical model can snap into this neighboring realization due to non-destructive elastic deformations of material. Shakiness can be seen as the limiting case where two realizations of a framework coincide; e.g. [2, 3].

The open problem in this context is the meaning of *closeness*, which is tackled in this article. In more detail, we present a method to measure the snapping capability (shortly called *snappability*) of a realization. The provided distance is of interest for practical applications, because it can be used in the early design phase of a framework to avoid snapping phenomena (e.g. engineering of truss structures) or to utilize them (e.g. multistable mechanisms and materials). The latter approach has received much attention in the last few years within a wide field of applications; ranging from origami structures (e.g. [4,5,6]) over mechanical metamaterials (e.g. [7,8,9]) to metastructures (e.g. [10]).

But the snappability also provides a distance to the next shaky configuration in the case of isostatic frameworks. Therefore this singularity-distance can also be used in the context of singularity-free path planing of robotic devices.

---

[1] A polygonal panel can be seen as a body with coplanar vertices according to [1].

1.1 Review and outline

In two recent conference articles [11,12] the author already started to investigate this topic. In [11] a first attempt towards the computation of the snappability of bar-joint frameworks was done based on the definition of Cauchy/Engineering strain. In [12] the author extended the approach to frameworks composed of bars and triangular panels. For this it was necessary to switch to the concept of Green-Lagrange strain, as the elastic strain energy of triangular panels using Cauchy/Engineering strain is not invariant under rotations. In the articles [11,12] the author restricted to planar examples; namely the trivial case of a triangular framework and the more sophisticated example of a pinned 3-legged planar parallel manipulator. In the paper at hand, we render the approach of [12] more precisely and generalize it to polygonal panels and polyhedra, respectively, and study some spatial frameworks, which already appear in existing literature on this topic reviewed next.

By the well-known technique of *deaveraging* (e.g. [3], [13, page 1604] and [14]) snapping frameworks can be constructed in any dimension $\mathbb{R}^d$. Moreover, for snapping bipartite frameworks in $\mathbb{R}^d$ an explicit result in terms of confocal hyperquadrics is known (cf. [3, page 112] under consideration of [15]). Most results are known for the dimension $d = 3$, which are as follows: There is a series of papers by Walter Wunderlich on snapping spatial structures (octahedra [16], closed 4R loops [17], antiprisms [18], icosahedra [19,20], dodecahedra [21]), which are reviewed in [22]. In this context also the paper [23] should be cited, where *buckling polyhedral surfaces* and *Siamese dipyramids* are introduced. Snapping structures are also related to so-called *model flexors*[2] (cf. [24]) as in some cases the model flexibility can be reasoned by the snapping through different realizations. Examples for this phenomenon are the so-called *four-horn* [25] or the already mentioned *Siamese dipyramid*. The latter are studied in more detail in [26], especially how minor relative variations on the edge lengths produce significant relative variations in the spatial shape. The authors of [26] also suggested estimates to quantify these intrinsic and extrinsic variations. Recently, a more general approach for estimating these kinds of quantities for arbitrary bar-joint frameworks was presented in [27], where inter alia also the Siamese dipyramid was studied as an example.

Beside the above reviewed mathematical studies on snapping frameworks, there are also the following application driven approaches. Their snapping behavior is studied by

(1) numerical simulations based on (a) finite element methods [7,8,9] or (b) force method approaches like [28] or a generalized displacement control method [4,5,6],

(2) theoretical approaches based on the variation of the total potential energy [9,10,29,30].

In contrast, our approach only relies on the total strain energy of the structure (i.e. no a priori assumptions on external loads have to be made) paving the way for the definition of the snappability, which only depends on the intrinsic framework geometry. Finally it should be noted, that a short review on approaches towards the computation of singular-distances is given in the section dealing with Stewart-Gough (SG) manipulators, which brings us straight to the outline of the paper.

After introducing notations and summarizing fundamentals of rigidity theory in Section 1.2, we present the underlying physical model of deformation in Section 2, which is used for building up the pseudometric on the space of intrinsic framework geometries in Section 3. Based on some theoretical considerations, we discuss the computation of the snappability and the singularity-distance in Sections 4 and 5, respectively, and demonstrate the presented methods in two examples. Afterward we adopt our theoretical results for the singularity-distance computation of SG platforms in Section 6, which is also closed by a practical example. Finally we conclude the paper in Section 7. Moreover, in Appendix A the Siamese dipyramid and the four-horn are studied, and the obtained results are compared with existing literature.

1.2 Notations and fundamentals of rigidity theory

A pin-jointed body-bar framework $G(\mathscr{K})$ consists of a knot set $\mathscr{K} = \left\{ V_1, \ldots, V_r, B_1^{d_1}(n_1), \ldots, B_q^{d_q}(n_q) \right\}$ and an 2-edge colored (green, red) graph G on $\mathscr{K}$. A knot $B_i^{d_i}(n_i)$ represents a body, where $d_i \in \{2,3\}$ gives the additional information if the body is a polyhedron ($\Leftrightarrow d_i = 3$) or a polygonal panel ($\Leftrightarrow d_i = 2$). Without loss of generality we can assume that $d_1 = \ldots = d_p = 2$ and $d_{p+1} = \ldots = d_q = 3$ for $1 \leq p \leq q$. The number n_i gives the number of vertices of the body B_i. A knot V_i corresponds to rotational/spherical joint linking bars. A green edge connecting two knots corresponds to a bar. A red edge is only allowed to connect two bodies and represents a pin-joint.

Due to the assumed global rigidity of the inner graph of a body we can replace each body by a globally rigid bar-joint subframework according to [1, page 437]. Note that the combinatorial characterization of global rigidity is only known for $\mathbb{R}^2$ (cf. [31]), but still open for $\mathbb{R}^3$ [1, page 450].

Remark 1. *The completeness of an inner graph is a sufficient condition for global rigidity (cf. [32]). This implies that the body $B_i^{d_i}(n_i)$ has to be convex as all $n_i(n_i - 1)/2$ edges are in the interior of the polyhedron (polygon) or on its boundary.*

Note that the globally rigid bar-joint subframework of a polygonal panel $B_i^2(n_i)$ is not infinitesimal rigid in $\mathbb{R}^3$ for $n_i > 3$ because every vertex can be infinitesimally flexed out of the plane spanned by the remaining $n_i - 1$ vertices. $\diamond$

---

[2]Mathematically these structures do not posses a continuous flexibility but due to free bendings without visible distortions of materials their physical models flex.

By replacing the bodies by globally rigid bar-joint subframeworks resulting from the inner graphs, we end up with a bar-joint framework $G_*(\mathcal{K}_*)$ which is equivalent to the given pin-jointed body-bar framework $G(\mathcal{K})$. This bar-joint framework $G_*(\mathcal{K}_*)$ can be used for defining the intrinsic geometry of the framework $G(\mathcal{K})$ in a mathematical rigorous way. For doing this, we introduce the following notation.

By denoting the vertices of the body $B_i^{d_i}(n_i)$ by $V_{s_i+1}, \ldots, V_{s_i+n_i}$ with $s_i = r + \sum_{j=1}^{i-1} n_j$ we get the set $\mathcal{K}_* = \{V_1, \ldots, V_w\}$ with $w = r + \sum_{j=1}^{q} n_j$. Moreover, we denote the edge connecting V_i to V_j by e_{ij} with $i < j$. Now we can fix the intrinsic metric of the framework $G_*(\mathcal{K}_*)$ (and therefore also of $G(\mathcal{K})$) by assigning a length $L_{ij} \in \mathbb{R}_{>0}$ to each edge e_{ij}. Moreover, we collect all these lengths in the b-dimensional vector $\mathbf{L} = (\ldots, L_{ij}, \ldots)^T$ of the space $\mathbb{R}^b$ of intrinsic framework metrics, where b gives the number of edges of the graph G_*. Finally we collect the indices ij of edges e_{ij} of $G_*(\mathcal{K}_*)$ which correspond to green edges of $G(\mathcal{K})$ in the set $\mathcal{G}$.

We denote a realization of the framework $G(\mathcal{K})$ and $G_*(\mathcal{K}_*)$ by $G(\mathbf{V})$ and $G_*(\mathbf{V})$, respectively, where the configuration of vertices $\mathbf{V} = (\mathbf{v}_1, \ldots, \mathbf{v}_w) \in \mathbb{R}^{wd}$ is composed by the coordinate vectors $\mathbf{v}_i = (x_i, y_i, z_i)^T$ for $d = 3$ and $\mathbf{v}_i = (x_i, y_i)^T$ for $d = 2$, respectively, of V_i for $i = 1, \ldots, w$.

Now we consider a realization $G_*(\mathbf{V})$ of the equivalent bar-joint framework $G_*(\mathcal{K}_*)$. In the rigidity community (e.g. [33]) each edge e_{ij} is assigned with a *stress (coefficient)* $\omega_{ij} \in \mathbb{R}$. For every knot V_i we can associate a so-called *equilibrium condition*

$$\sum_{i<j\in N_i} \omega_{ij}(\mathbf{v}_i - \mathbf{v}_j) + \sum_{i>j\in N_i} \omega_{ji}(\mathbf{v}_i - \mathbf{v}_j) = \mathbf{o} \tag{1}$$

where $\mathbf{o}$ denotes the d-dimensional zero-vector and N_i the knot neighborhood of V_i; i.e. the index set of knots $\in \mathcal{K}_*$ connected with V_i by bars. If for all w knots this condition is fulfilled, then the b-dimensional stress-vector $\omega = (\ldots, \omega_{ij}, \ldots)^T$ is referred as *self-stress* (or *equilibrium stress*).

Algebraic approach to rigidity theory. The relation that two elements of the knot set are edge-connected can also be expressed algebraically. They are either quadratic constraints resulting from the squared distances of vertices (implied by a green edge) or they are linear conditions, which are stemming from the identification of vertices (implied by a red edge) or the elimination of isometries[3]. In total this results in a system of n algebraic equations $c_1 = 0, \ldots, c_n = 0$ in m unknowns[4], which constitute an algebraic variety A.

If $A(c_1, \ldots, c_n)$ is positive-dimensional then the framework is flexible; otherwise rigid. The framework is called minimally rigid (isostatic) if the removal of any algebraic constraint (resulting from an edge) will make the framework flexible. In this case $m = n$ has to hold. Rigid frameworks, which are not isostatic, are called *overbraced* or *overconstrained* ($n > m$). Note that there is also a combinatorial characterization of isostaticity for generic frameworks of dimension 2 according to the work of Laman [34], but for dimension 3 this is still an open problem.

If $A(c_1, \ldots, c_n)$ is zero-dimensional, then each real solution corresponds to a realization $G(\mathbf{V}_i)$ of the framework for $i = 1, \ldots, k$. If there is exactly one real solution, then the framework is called globally rigid. But one can also consider the complex solutions of the set of *realization equations* $c_1, \ldots, c_n$ resulting in complex knot configurations $\mathbf{V}_i$ with $i = k+1, \ldots, k+2f$ and $f \in \mathbb{N}^*$ as they always appear in pairs. According to [35] they imply complex realizations $G(\mathbf{V}_i)$.

We can compute in a realization the tangent-hyperplane to each of the hypersurfaces $c_i = 0$ in $\mathbb{R}^m$ for $i = 1, \ldots, n$. Note that this is always possible as all hypersurfaces are either hyperplanes or regular hyperquadrics. The normal vectors of these tangent-hyperplanes constitute the columns of a $m \times n$ matrix $\mathbf{R}_{G(\mathbf{V})}$, which is also known as *rigidity matrix* of the realization $G(\mathbf{V})$. If its rank is m then the realization is infinitesimal rigid otherwise it is infinitesimal flexible; i.e. the hyperplanes have a positive-dimensional affine subspace in common. Therefore the intersection multiplicity of the n hypersurfaces is at least two in a shaky realization. As a consequence shakiness (of order one[5]) can also be seen as the limiting case where two realizations of a framework coincide [2, 3, 22].

Clearly, by using the rank condition $rk(\mathbf{R}_{G(\mathbf{V})}) < m$ one can also characterize all shaky realizations $G(\mathbf{V})$ algebraically by the affine variety $A(J)$ – which is referred as shakiness variety – where J denotes the ideal generated by all minors of $\mathbf{R}_{G(\mathbf{V})}$ of order $m \times m$. Let us assume that the polynomials $g_1, \ldots, g_\gamma$ form the Gröbner basis of the ideal J. Note that for minimally rigid framework $\gamma = 1$ holds, where the infinitesimal flexibility is given by $g_1 : \det(\mathbf{R}_{G(\mathbf{V})}) = 0$. Another approach towards this so-called *pure condition* in terms of brackets is given in [36].

2 Physical model of deformation

The snappability index presented in this paper is based on the physical model of deformation relying on the concept of Green-Lagrange strain, which is reduced to its geometric core by eliminating the influence of material properties. In order

---

[3]This are 6 linear constraints for $d = 3$ and 3 linear constraints for $d = 2$.

[4]Note that for bar-joint frameworks this number equals wd, where w is the number of vertices.

[5]Each additional coinciding realization raises the order of the infinitesimal flexibility by one [2].

to do so, we make the following assumption.

Assumption 1. *All bars and bodies of the framework are made of the same homogeneous isotropic material, which is non-auxetic; i.e. the Poisson ratio $v \in [0, 1/2]$, and has a positive Young modulus $E > 0$.*

2.1 The relation between stress and strain

Due to the fact that the elastic deformations during the process of snapping are expected to be small, we can apply Hooke's law. As a consequence, the relation between applied stresses and resulting strains is a linear one, which can be given for the spatial case by

$$\underbrace{\begin{pmatrix} \varepsilon_x \\ \varepsilon_y \\ \varepsilon_z \\ \gamma_{xy} \\ \gamma_{xz} \\ \gamma_{yz} \end{pmatrix}}_{\mathbf{e}_3} = \frac{1}{E} \underbrace{\begin{pmatrix} 1 & -v & -v & 0 & 0 & 0 \\ -v & 1 & -v & 0 & 0 & 0 \\ -v & -v & 1 & 0 & 0 & 0 \\ 0 & 0 & 0 & 2(1+v) & 0 & 0 \\ 0 & 0 & 0 & 0 & 2(1+v) & 0 \\ 0 & 0 & 0 & 0 & 0 & 2(1+v) \end{pmatrix}}_{=:\mathbf{D}_3(v)} \begin{pmatrix} \delta_x \\ \delta_y \\ \delta_z \\ \tau_{xy} \\ \tau_{xz} \\ \tau_{yz} \end{pmatrix} \tag{2}$$

where δ_i denotes the normal stress in i-direction and ε_i its corresponding normal strain with $i \in \{x, y, z\}$. Moreover, τ_{ij} denotes the shear stress in the ij-plane and γ_{ij} its corresponding shear strain with $i \neq j$ and $i, j \in \{x, y, z\}$.

In the case of planar stress (xy-plane) the shear stresses τ_{xz} and τ_{yz} are zero as well as the normal stress δ_z. Then Eq. (2) simplifies to:

$$\underbrace{\begin{pmatrix} \varepsilon_x \\ \varepsilon_y \\ \gamma_{xy} \end{pmatrix}}_{\mathbf{e}_2} = \frac{1}{E} \underbrace{\begin{pmatrix} 1 & -v & 0 \\ -v & 1 & 0 \\ 0 & 0 & 2(1+v) \end{pmatrix}}_{=:\mathbf{D}_2(v)} \begin{pmatrix} \delta_x \\ \delta_y \\ \tau_{xy} \end{pmatrix}. \tag{3}$$

In the case of a bar (in x-direction) the relation reduces to $\varepsilon_x = D_1 \delta_x$ with $D_1 := \frac{1}{E}$.

For the later done computation of the elastic strain energies we need the inverse relations, which map the strains to the stresses. This can be obtained by inverting D_1, $\mathbf{D}_2$ and $\mathbf{D}_3$, respectively. D_1 does not depend on Poisson's ratio v and its inverse reads as $D_1^{-1} = E$.

As $\mathbf{D}_2$ is regular for all possible Poisson ratios $v \in [0, 1/2]$, we can always compute

$$\mathbf{D}_2^{-1}(v) = E \begin{pmatrix} \frac{1}{1-v^2} & \frac{v}{1-v^2} & 0 \\ \frac{v}{1-v^2} & \frac{1}{1-v^2} & 0 \\ 0 & 0 & \frac{1}{2(1+v)} \end{pmatrix} \quad \text{for} \quad 0 \leq v \leq \frac{1}{2}. \tag{4}$$

For the spatial case, $\mathbf{D}_3^{-1}(v)$ is only not defined if v equals the upper border of $\frac{1}{2}$, thus we get:

$$\mathbf{D}_3^{-1}(v) = E \begin{pmatrix} \frac{v-1}{2v^2+v-1} & \frac{-v}{2v^2+v-1} & \frac{-v}{2v^2+v-1} & 0 & 0 & 0 \\ \frac{-v}{2v^2+v-1} & \frac{v-1}{2v^2+v-1} & \frac{-v}{2v^2+v-1} & 0 & 0 & 0 \\ \frac{-v}{2v^2+v-1} & \frac{-v}{2v^2+v-1} & \frac{v-1}{2v^2+v-1} & 0 & 0 & 0 \\ 0 & 0 & 0 & \frac{1}{2(1+v)} & 0 & 0 \\ 0 & 0 & 0 & 0 & \frac{1}{2(1+v)} & 0 \\ 0 & 0 & 0 & 0 & 0 & \frac{1}{2(1+v)} \end{pmatrix} \quad \text{for} \quad 0 \leq v < \frac{1}{2}. \tag{5}$$

For $v = \frac{1}{2}$ we compute the Moore-Penrose pseudo inverse of $\mathbf{D}_3$ which yields:

$$\mathbf{D}_3^{-1}(\tfrac{1}{2}) = E \begin{pmatrix} \frac{4}{9} & -\frac{2}{9} & -\frac{2}{9} & 0 & 0 & 0 \\ -\frac{2}{9} & \frac{4}{9} & -\frac{2}{9} & 0 & 0 & 0 \\ -\frac{2}{9} & -\frac{2}{9} & \frac{4}{9} & 0 & 0 & 0 \\ 0 & 0 & 0 & \frac{1}{3} & 0 & 0 \\ 0 & 0 & 0 & 0 & \frac{1}{3} & 0 \\ 0 & 0 & 0 & 0 & 0 & \frac{1}{3} \end{pmatrix}. \tag{6}$$

2.2 Strain energy according to Green-Lagrange

The study of the deformation of a polyhedron is based on the deformation of tetrahedra, which also play a central role in the stress analysis within the finite element method (e.g. see [37, Chapter 6]). The strain computation for 3-simplices according to Green-Lagrange is outlined next (e.g. see [38, Section 2.4.2]).

Let V_a, V_b, V_c, V_d denote the vertices of the tetrahedron in the given undeformed configuration and V_a', V_b', V_c', V_d' in the deformed one. Then there exists a uniquely defined 3×3 matrix $\mathbf{A}$ which has the property

$$\mathbf{A}(\widehat{\mathbf{v}}_b - \widehat{\mathbf{v}}_a) = \widehat{\mathbf{v}}_b' - \widehat{\mathbf{v}}_a', \qquad \mathbf{A}(\widehat{\mathbf{v}}_c - \widehat{\mathbf{v}}_a) = \widehat{\mathbf{v}}_c' - \widehat{\mathbf{v}}_a', \qquad \mathbf{A}(\widehat{\mathbf{v}}_d - \widehat{\mathbf{v}}_a) = \widehat{\mathbf{v}}_d' - \widehat{\mathbf{v}}_a', \tag{7}$$

where $\widehat{\mathbf{v}}_i$ (resp. $\widehat{\mathbf{v}}_i'$) is a 3-dimensional vector of V_i (resp. V_i') for $i \in \{a,b,c,d\}$ with respect to a Cartesian frame $\mathscr{F}$ (resp. $\mathscr{F}'$) attached to the undeformed (resp. deformed) tetrahedron. The Cartesian frame $\mathscr{F}$ can always be chosen in a way that its origin equals V_a, the vertex V_b is located on its positive x-axis and V_c is located in the xy-plane with a positive y coordinate; i.e.

$$\widehat{\mathbf{v}}_a = (0,0,0)^T, \quad \widehat{\mathbf{v}}_b = (x_b, 0, 0)^T, \quad \widehat{\mathbf{v}}_c = (x_c, y_c, 0)^T, \quad \widehat{\mathbf{v}}_d = (x_d, y_d, z_d)^T, \tag{8}$$

with $x_b > 0$ and $y_c > 0$. Similar considerations can be done for the Cartesian frame $\mathscr{F}'$ with respect to the tetrahedron V_a', V_b', V_c', V_d' ending up with exactly the same coordinatization as above but only primed. Then the normal strains and the shear strains can be computed as

$$\begin{pmatrix} \varepsilon_x & \frac{\gamma_{xy}}{2} & \frac{\gamma_{xz}}{2} \\ \frac{\gamma_{xy}}{2} & \varepsilon_y & \frac{\gamma_{yz}}{2} \\ \frac{\gamma_{xz}}{2} & \frac{\gamma_{yz}}{2} & \varepsilon_z \end{pmatrix} = \frac{1}{2}\left(\mathbf{A}^T\mathbf{A} - \mathbf{I}\right). \tag{9}$$

Reassembling these quantities in the vector $\mathbf{e}_3$ (cf. Eq. (2)) the elastic strain energy of the deformation can be calculated as

$$U_{abcd} = \text{Vol}_{abcd}\,\tfrac{1}{2}\mathbf{e}_3^T \mathbf{D}_3^{-1}(v)\mathbf{e}_3 \tag{10}$$

where Vol_{abcd} denotes the volume of the undeformed tetrahedron and $\mathbf{D}_3^{-1}(v)$ the stress/strain matrix (constitutive matrix) from Eq. (5) and Eq. (6), respectively.

The same procedure can be done for the computation of the elastic strain energy U_{abc} of a triangular panel with vertices V_a, V_b and V_c, which is outlined in detail in [12]. As final formula we obtain in this case:

$$U_{abc} = \text{Vol}_{abc}\,\tfrac{1}{2}\mathbf{e}_2^T \mathbf{D}_2^{-1}(v)\mathbf{e}_2 \tag{11}$$

where $\mathbf{D}_2^{-1}(v)$ denotes the stress/strain matrix from Eq. (4) and Vol_{abc} the volume of the undeformed panel, which can be computed as the product of the triangle's area Area_{abc} and the panel height h_{abc}. For a bar with end-points V_a and V_b we end up with the following simple expression:

$$U_{ab} = \frac{E\,\text{Vol}_{ab}}{8L_{ab}^4}(L_{ab}'^2 - L_{ab}^2)^2 \tag{12}$$

where Vol_{ab} denotes the volume of the undeformed bar, which can be computed as the product of the length L_{ab} of the undeformed bar and its cross-sectional area Area_{ab}. The deformed bar length is given by L_{ab}'.

3 A pseudometric on the space of intrinsic framework metrics

In this section we set up a pseudometric on the space of intrinsic framework metrics, which is based on the total strain energy density of the framework, because in this way the distance is invariant under scaling (change of unit length). Moreover, it allows to compare pin-jointed body-bar frameworks differing in the number of knots, the combinatorial structure and intrinsic metric.

3.1 The strain energy density of a framework

We assume that the intrinsic metric of the framework $G(\mathcal{K})$ is given by the edge-length vector $\mathbf{L} = (\ldots, L_{ij}, \ldots)^T \in \mathbb{R}^b$ of the equivalent framework $G_*(\mathcal{K}_*)$. In the same way the intrinsic metric of the deformed framework is determined by $\mathbf{L}' = (\ldots, L'_{ij}, \ldots)^T \in \mathbb{R}^b$. As the strain energy of a polyhedron (polygonal panel) depends on its tetrahedralization[6] (triangulation[7]) we compute the strain energy over all tetrahedra of the polyhedron (triangles of the polygonal panel). To do so, we define the index set $\mathcal{C}_i$ containing all index 4-tuple $abcd$ (3-tuple abc) with $a < b < c < d$ (with $a < b < c$) of non-degenerated[8] tetrahedra (triangles) within a polyhedron $B_i^3(n_i)$ (polygonal panel $B_i^2(n_i)$). Using this notation we can formulate the strain energy density within the next lemma.

Lemma 1. *The strain energy density of a pin-jointed body-bar framework given by*

$$u(\mathbf{L}') := \frac{\sum_{ab \in \mathcal{G}} U_{ab}(\mathbf{L}') + \sum_{i=1}^{p} Vol(B_i^2) \left[\frac{\sum_{abc \in \mathcal{C}_i} U_{abc}(\mathbf{L}')}{\sum_{abc \in \mathcal{C}_i} Vol_{abc}} \right] + \sum_{j=p+1}^{q} Vol(B_j^3) \left[\frac{\sum_{abcd \in \mathcal{C}_j} U_{abcd}(\mathbf{L}')}{\sum_{abcd \in \mathcal{C}_j} Vol_{abcd}} \right]}{\sum_{ab \in \mathcal{G}} Vol_{ab} + \sum_{i=1}^{p} Vol(B_i^2) + \sum_{j=p+1}^{q} Vol(B_j^3)} \tag{13}$$

is defined by the intrinsic metric $\mathbf{L}$ of the undeformed framework, the cross-sectional areas $Area_{ab}$ of its bars, the panel heights h_{abc} and the material constants E and v. The argument of the density function is given by the intrinsic metric $\mathbf{L}'$ of the deformed framework. It is a fourth order polynomial with respect to the variables L'_{ij} which only appear with even powers.

Proof: We prove this lemma by investigating each summand in the numerator of Eq. (13) for the stated properties. As the energy functions differ for bars, triangular panels and tetrahedra, we have to split up the proof into these three cases:

- *Bar:* For bars this result follows directly from Eq. (12).
- *Triangular panel:* We choose a planar Cartesian frame $\mathcal{F}$ in a way that the coordinates of the triangle V_a, V_b, V_c read as $\hat{\mathbf{v}}_a = (0,0)^T$, $\hat{\mathbf{v}}_b = (x_b, 0)^T$ and $\hat{\mathbf{v}}_c = (x_c, y_c)^T$ with

$$x_b = L_{ab}, \quad x_c = \frac{L_{ab}^2 + L_{ac}^2 - L_{bc}^2}{2L_{ab}}, \quad y_c = \frac{\sqrt{(L_{ab} + L_{ac} + L_{bc})(L_{ab} - L_{ac} + L_{bc})(L_{ab} + L_{ac} - L_{bc})(L_{ac} + L_{bc} - L_{ab})}}{2L_{ab}} \tag{14}$$

  where the coordinate y_c can have positive or negative sign for planar frameworks depending on the orientation of the triangle V_a, V_b, V_c. For spatial frameworks one can always assume a positive sign. Similar considerations can be done for the planar Cartesian frame $\mathcal{F}'$ with respect to the triangle V'_a, V'_b, V'_c ending up with exactly the same coordinatization as above but only primed. Inserting these coordinates of the six vectors $\hat{\mathbf{v}}_a, \hat{\mathbf{v}}_b, \hat{\mathbf{v}}_c, \hat{\mathbf{v}}'_a, \hat{\mathbf{v}}'_b, \hat{\mathbf{v}}'_c$ into Eq. (11) shows the result for triangular panels by taking into account that the area $Area_{abc}$ of the triangle can be computed by Heron's formula. Note that the obtained expression is independent of the signs of the y-coordinates of $\hat{\mathbf{v}}_c$ and $\hat{\mathbf{v}}'_c$.
- *Tetrahedron:* We choose the same Cartesian frame $\mathcal{F}$ as in Section 2.2 which implies the coordinatization of the tetrahedron V_a, V_b, V_c, V_d given in Eq. (8) with x_b, x_c and y_c from Eq. (14) and

$$x_d = \frac{L_{ab}^2 + L_{ad}^2 - L_{bd}^2}{2L_{ab}}, \quad y_d = \frac{L_{ab}^2 L_{ac}^2 + L_{ab}^2 L_{ad}^2 + L_{ab}^2 L_{bc}^2 + L_{ab}^2 L_{bd}^2 - 2L_{ab}^2 L_{cd}^2 - L_{ac}^2 L_{ad}^2 + L_{ac}^2 L_{bd}^2 + L_{ad}^2 L_{bc}^2 - L_{bc}^2 L_{bd}^2 - L_{ab}^4}{2L_{ab}\sqrt{(L_{ab} + L_{ac} + L_{bc})(L_{ab} - L_{ac} + L_{bc})(L_{ab} + L_{ac} - L_{bc})(L_{ac} + L_{bc} - L_{ab})}}$$

$$z_d = (-L_{ab}^4 L_{cd}^2 - L_{ab}^2 L_{ac}^2 L_{bc}^2 + L_{ab}^2 L_{ac}^2 L_{bd}^2 + L_{ab}^2 L_{ac}^2 L_{cd}^2 + L_{ab}^2 L_{ad}^2 L_{bc}^2 - L_{ab}^2 L_{ad}^2 L_{bd}^2 + L_{ab}^2 L_{ad}^2 L_{cd}^2 + L_{ab}^2 L_{bc}^2 L_{cd}^2 + L_{ab}^2 L_{bd}^2 L_{cd}^2 - L_{ab}^2 L_{cd}^4 - L_{ac}^4 L_{bd}^2 +$$
$$L_{ac}^2 L_{ad}^2 L_{bc}^2 + L_{ac}^2 L_{ad}^2 L_{bd}^2 - L_{ac}^2 L_{ad}^2 L_{cd}^2 + L_{ac}^2 L_{bc}^2 L_{bd}^2 - L_{ac}^2 L_{bd}^4 + L_{ac}^2 L_{bd}^2 L_{cd}^2 - L_{ad}^4 L_{bc}^2 - L_{ad}^2 L_{bc}^4 + L_{ad}^2 L_{bc}^2 L_{bd}^2 + L_{ad}^2 L_{bc}^2 L_{cd}^2 - L_{bc}^2 L_{bd}^2 L_{cd}^2)^{1/2} / $$
$$\sqrt{(L_{ab} + L_{ac} + L_{bc})(L_{ab} - L_{ac} + L_{bc})(L_{ab} + L_{ac} - L_{bc})(L_{ac} + L_{bc} - L_{ab})} \tag{15}$$

  where the coordinate z_d can have positive or negative sign depending on the orientation of the tetrahedron V_a, V_b, V_c, V_d. We get the same coordinatization for the tetrahedron V'_a, V'_b, V'_c, V'_d as above but only primed. Inserting these eight vectors

---

[6]Decomposition into a set of disjoint tetrahedra without adding new vertices.

[7]Decomposition into a set of disjoint triangles without adding new vertices.

[8]The tetrahedron (triangle) does not degenerate into a plane (line). Note that $\#\mathcal{C}_i = (n_i - 3)(n_i - 2)(n_i - 1)n_i/24$ ($\#\mathcal{C}_i = (n_i - 2)(n_i - 1)n_i/6$) holds if the polyhedron (polygonal panel) is strictly convex.

$\widehat{\mathbf{v}}_a, \widehat{\mathbf{v}}_b, \widehat{\mathbf{v}}_c, \widehat{\mathbf{v}}_d, \widehat{\mathbf{v}}'_a, \widehat{\mathbf{v}}'_b, \widehat{\mathbf{v}}'_c, \widehat{\mathbf{v}}'_d$ into Eq. (10) under consideration that Vol_{abcd} can be computed by the Cayley-Menger determinant shows the stated result. Note that the obtained expression is independent of the sign of the z-coordinate of $\widehat{\mathbf{v}}_d$ and $\widehat{\mathbf{v}}'_d$. Moreover, it should be mentioned that the obtained polynomial is homogenous of degree 4 in L'_{ij} for $\nu = 1/2$. $\qquad\square$

Remark 2. *Concerning Lemma 1 the following should be noted:*

⋆ *The expressions given in the square brackets of Eq. (13) can be seen as the mean densities of the polygonal panels and polyhedra, respectively.*

⋆ *Note that the height h_{abc} of each triangular panel belonging to $B_i^2(n_i)$ equals the height h_i of $B_i^2(n_i)$.*

⋆ *Due to Lemma 1 the formula for $u(\mathbf{L}')$ can be written in matrix formulation as $u(\mathbf{Q}') = \mathbf{Q}'^T \mathbf{M} \mathbf{Q}'$ where $\mathbf{M}$ is a symmetric $(b+1)$-matrix and $\mathbf{Q}' := (1, \ldots, Q'_{ij}, \ldots)^T$ is composed of the b squared edge lengths $Q'_{ij} := L'^2_{ij}$ and the number 1.* $\qquad\diamond$

3.2 Definition of the pseudometric

The pseudometric on the space $\mathbb{R}^b$ of intrinsic framework metrics is defined within the next lemma:

Lemma 2. *The following function*

$$d : \mathbb{R}^b \times \mathbb{R}^b \to \mathbb{R}_{\geq 0} \quad with \quad (\mathbf{L}', \mathbf{L}'') \mapsto d(\mathbf{L}', \mathbf{L}'') := \frac{|u(\mathbf{L}') - u(\mathbf{L}'')|}{E} \tag{16}$$

is a pseudometric on the b-dimensional space of intrinsic framework metrics given by $\mathbf{L}'$ and $\mathbf{L}''$, respectively. Moreover, the pseudometric does not depend on the choice of E.

Proof: One has to check the axioms for a pseudometric

$$(1)\ d(\mathbf{L}', \mathbf{L}'') \geq 0, \quad (2)\ d(\mathbf{L}', \mathbf{L}') = 0, \quad (3)\ d(\mathbf{L}', \mathbf{L}'') = d(\mathbf{L}'', \mathbf{L}'), \quad (4)\ d(\mathbf{L}', \mathbf{L}''') \leq d(\mathbf{L}', \mathbf{L}'') + d(\mathbf{L}'', \mathbf{L}'''), \tag{17}$$

which is a trivial task and remains to the reader.

Due to Assumption 1, Young's modulus E factors out of the density $u(\mathbf{L}')$. Therefore it factors out of the numerator of the distance function and cancels with the numerator. $\qquad\square$

From Lemma 1 it is clear that the pseudodistance of Eq. (16) does not only depend on the intrinsic metric $\mathbf{L}$ of the undeformed framework but also on the cross-sectional areas of the bars and the heights of the panels, which are needed for the computation of their volumes. In the following section we fix these parameters by relating them to the intrinsic geometry of the undeformed framework.

3.2.1 Geometric motivated volumetric dimensioning of bars and panels

As mentioned in Section 1.2 each pin-jointed body-bar framework $G(\mathcal{K})$ can be replaced by an equivalent bar-joint framework $G_*(\mathcal{K}_*)$. In order to ensure a fair comparability of both frameworks, we came up with the following assumption.

Assumption 2. *The frameworks $G(\mathcal{K})$ and $G_*(\mathcal{K}_*)$ have the same volume; i.e. they are built from the same amount of material. Moreover, we assume that all bars have the same cross-sectional area noted by $\mathrm{Area}_\varnothing$.*

We start with the volumes of the polyhedra $\mathrm{Vol}\left(B_j^3(n_j)\right)$, which are already determined by $\mathbf{L}$, and compute $\mathrm{Area}_\varnothing$ as

$$\mathrm{Area}_\varnothing := \frac{\sum_{j=p+1}^q \mathrm{Vol}\left(B_j^3(n_j)\right)}{\sum_{j=p+1}^q \sum_{ab \in \mathscr{I}_j} W_{ab} L_{ab}} \tag{18}$$

where $\mathscr{I}_j$ is the index set of all pairs of vertices belonging to an edge of the inner graph of the polyhedron $B_j^3(n_j)$. Moreover, the weight factor W_{ab} is one over the number of bodies hinged along the corresponding bar[9].

Now having $\mathrm{Area}_\varnothing$ one can also compute the height h_i of the polygonal panel $B_i^2(n_i)$ over the bar-joint subframework equivalent to $B_i^2(n_i)$ as:

$$h_i := \frac{\mathrm{Area}_\varnothing \sum_{ab \in \mathscr{I}_i} W_{ab} L_{ab}}{\mathrm{Area}\left(B_i^2(n_i)\right)} \tag{19}$$

---

[9]If the bar does not hinge bodies, then the weight factor is one.

where $\mathscr{I}_i$ is the index set of all pairs of vertices belonging to an edge of the inner graph of the polygonal panel $B_i^2(n_i)$. In the case that the framework does not contain any polyhedra, then we can compute h_i in the same way but depending on the unknown $\text{Area}_\varnothing$. In this case it can easily be seen that $\text{Area}_\varnothing$ factors out in the numerator as well as in the denominator of Eq. (13). Therefore Eq. (16) does not depend on $\text{Area}_\varnothing$. This also holds if the given framework is already a bar-joint framework.

3.2.2 Geometric motivated choice of Poisson's ratio

Under consideration of Section 3.2.1 the pseudometric d only depends on Poisson's ratio ν beside the intrinsic metric $\mathbf{L}$ of the undeformed framework. From the geometric point of view the most satisfying choice is $\nu = 1/2$ as in this case the framework deforms at constant volume, which is also known as an *isochoric* deformation. This does not pose any problems for a bar or triangular panel, as one can always define the cross-sectional area Area'_{ab} of the deformed bar by Vol_{ab}/L'_{ab} and a height h'_{abc} of the deformed panel by $\text{Vol}_{abc}/\text{Area}'_{abc}$, respectively, where Area'_{abc} is the area of the deformed triangle V'_a, V'_b, V'_c. But for each tetrahedron we get the additional condition that $\text{Vol}_{abcd} = \text{Vol}'_{abcd}$ holds, which fits very well into our theory for the following reason: The Moore-Penrose pseudo inverse of $\mathbf{D}_3^{-1}(\frac{1}{2})$ of Eq. (6) would imply that there exists a 1-dimensional set of strains $(\alpha, \alpha, \alpha, 0, 0, 0)$ with $\alpha \in \mathbb{R}$ yielding zero stresses, which cannot be the case[10]. Plugging the entries of this strain vector into Eq. (9) shows that it results from an equiform motion (Euclidean motion plus a scaling). But an equiform motion keeping the volume fixed has to be an Euclidean motion ($\Leftrightarrow \alpha = 0$), which does not imply any stress. Hence, the condition $\text{Vol}_{abcd} = \text{Vol}'_{abcd}$ resolves also the problem arising from the singularity of the stress/strain matrix given in Eq. (6). Therefore one is only allowed to compute the pseudodistance of Eq. (16) for $\nu = 1/2$ if $\text{Vol}_{abcd} = \text{Vol}'_{abcd}$ holds for all $abcd \in \mathscr{C}_j$ for $j = p+1, \ldots, q$.

Clearly, theoretically one can also use another Poisson ratio $0 \le \nu < 1/2$ but in this paper we focus on the more sophisticated problem assuming constant volume under the deformation. A consequence of the constant volume deformation is that Eq. (13) cannot only be seen as the energy per volume, which has to be applied to the given framework to reach the deformed configuration but as the energy per volume which is stored in the deformed framework.

Remark 3. *If one does not want to use the Poisson ratio $\nu = 1/2$, then one is confronted to make a choice within the interval $[0; 1/2[$. One can circumvent the arbitrariness in the choice by determining ν within a constrained optimization $(0 \le \nu < 1/2)$ in such a way that the distance of Eq. (16) is minimal. The disadvantage of this approach is that the triangular inequality of Eq. (17) cannot longer be guaranteed thus the pseudometric degenerates to a so-called premetric.* $\diamond$

Finally, it should be noted that the results of the next sections are general ones; i.e. the assumptions done in Section 3.2.1 and 3.2.2 are not necessary for their validity.

4 Local and global snappability

If we want to compute the distance between $\mathbf{L}$ and $\mathbf{L}'$ then the pseudometric $d(\mathbf{L}, \mathbf{L}')$ simplifies to $u(\mathbf{L}')/E$ as this function is positive-definite, which is clear from the underlying physical interpretation but one can also prove this mathematically by decomposing it into a sum of squares (see e.g. [39]).

As we can replace L'_{ij} in $u(\mathbf{L}')$ by $\|\mathbf{v}'_i - \mathbf{v}'_j\|$ the function u can be computed in dependence of $\mathbf{V}'$; i.e. $u(\mathbf{V}')$.

Theorem 1. *For $0 \le \nu < 1/2$ the critical points of the total elastic strain energy density $u(\mathbf{V}')$ of a pin-jointed body-bar framework correspond to realizations $G_*(\mathbf{V}')$ of the equivalent bar-joint framework that are either undeformed or deformed with a non-zero self-stress. This also holds for $\nu = 1/2$ under the side conditions of constant tetrahedral volumes.*

Proof: The system of equations characterizing the critical points of $u(\mathbf{V}')$ reads as follows:

$$\nabla_i u(\mathbf{V}') = \mathbf{o} \quad \text{with} \quad \begin{cases} \nabla_i u(\mathbf{V}') = \left(\frac{\partial u}{\partial x'_i}, \frac{\partial u}{\partial y'_i} \right) & \text{for } d = 2 \\ \nabla_i u(\mathbf{V}') = \left(\frac{\partial u}{\partial x'_i}, \frac{\partial u}{\partial y'_i}, \frac{\partial u}{\partial z'_i} \right) & \text{for } d = 3 \end{cases} \tag{20}$$

with $i = 1, \ldots, w$, where $(x'_i, y'_i)^T$ and $(x'_i, y'_i, z'_i)^T$ is the coordinate vector of $\mathbf{v}'_i$ for the planar and spatial case, respectively. Due to the sum rule for derivatives we only have to investigate ∇_i of the following three functions: $U_{ab}(\mathbf{v}'_a, \mathbf{v}'_b)$ of Eq. (12), $U_{abc}(\mathbf{v}'_a, \mathbf{v}'_b, \mathbf{v}'_c)$ given in Eq. (11) and $U_{abcd}(\mathbf{v}'_a, \ldots, \mathbf{v}'_d)$ of Eq. (10), respectively.

1. Due to $\nabla_a U_{ab}(\mathbf{v}'_a, \mathbf{v}'_b) = \frac{\text{Area}_{ab}(L'^2_{ab} - L^2_{ab})}{2L^3_{ab}} (\mathbf{v}'_a - \mathbf{v}'_b)$ Theorem 1 is valid for frameworks, which only consist of bars, as $\nabla_a u(\mathbf{V}')$ can be written in the form of Eq. (1) with $\omega_{ab} = \frac{\text{Area}_{ab}(L'^2_{ab} - L^2_{ab})}{2L^3_{ab}}$.

---

[10]In fact the converse is true, that for $\nu = \frac{1}{2}$ there is no strain for uniform stresses.

2. If polygonal panels are involved we consider a representative triangular panel with vertices V_a, V_b, V_c and compute $\nabla_a U_{abc}(\mathbf{v}'_a, \mathbf{v}'_b, \mathbf{v}'_c)$, $\nabla_b U_{abc}(\mathbf{v}'_a, \mathbf{v}'_b, \mathbf{v}'_c)$ and $\nabla_c U_{abc}(\mathbf{v}'_a, \mathbf{v}'_b, \mathbf{v}'_c)$. Straight forward symbolic computations (e.g. using Maple) show that the following system of equations

$$
\begin{aligned}
\omega_{ab}(\mathbf{v}'_a - \mathbf{v}'_b) + \omega_{ac}(\mathbf{v}'_a - \mathbf{v}'_c) - \nabla_a U_{abc}(\mathbf{v}'_a, \mathbf{v}'_b, \mathbf{v}'_c) &= \mathbf{o} \\
\omega_{ab}(\mathbf{v}'_b - \mathbf{v}'_a) + \omega_{bc}(\mathbf{v}'_b - \mathbf{v}'_c) - \nabla_b U_{abc}(\mathbf{v}'_a, \mathbf{v}'_b, \mathbf{v}'_c) &= \mathbf{o} \\
\omega_{ac}(\mathbf{v}'_c - \mathbf{v}'_a) + \omega_{bc}(\mathbf{v}'_c - \mathbf{v}'_b) - \nabla_c U_{abc}(\mathbf{v}'_a, \mathbf{v}'_b, \mathbf{v}'_c) &= \mathbf{o}
\end{aligned}
\tag{21}
$$

which is overdetermined[11], has a unique solution for ω_{ab}, ω_{ac} and ω_{bc} if V'_a, V'_b, V'_c generate a triangle. If these points are collinear we even get a positive dimensional solution set. Hence, one can replace $\nabla_a U_{abc}(\mathbf{v}'_a, \mathbf{v}'_b, \mathbf{v}'_c)$ by a linear combination $\omega_{ab}(\mathbf{v}'_a - \mathbf{v}'_b) + \omega_{ac}(\mathbf{v}'_a - \mathbf{v}'_c)$ where the coefficients ω_{ab} and ω_{ac} are compatible with the other equations of (21).

3. If bodies are involved we consider a representative tetrahedron with vertices V_a, V_b, V_c, V_d and compute $\nabla_a U_{abcd}(\mathbf{v}'_a, \ldots, \mathbf{v}'_d)$, $\nabla_b U_{abcd}(\mathbf{v}'_a, \ldots, \mathbf{v}'_d)$, $\nabla_c U_{abcd}(\mathbf{v}'_a, \ldots, \mathbf{v}'_d)$ and $\nabla_d U_{abcd}(\mathbf{v}'_a, \ldots, \mathbf{v}'_d)$. Now we are faced with the system of equations

$$
\begin{aligned}
\omega_{ab}(\mathbf{v}'_a - \mathbf{v}'_b) + \omega_{ac}(\mathbf{v}'_a - \mathbf{v}'_c) + \omega_{ad}(\mathbf{v}'_a - \mathbf{v}'_d) - \nabla_a U_{abcd}(\mathbf{v}'_a, \ldots, \mathbf{v}'_d) &= \mathbf{o} \\
\omega_{ab}(\mathbf{v}'_b - \mathbf{v}'_a) + \omega_{bc}(\mathbf{v}'_b - \mathbf{v}'_c) + \omega_{bd}(\mathbf{v}'_b - \mathbf{v}'_d) - \nabla_b U_{abcd}(\mathbf{v}'_a, \ldots, \mathbf{v}'_d) &= \mathbf{o} \\
\omega_{ac}(\mathbf{v}'_c - \mathbf{v}'_a) + \omega_{bc}(\mathbf{v}'_c - \mathbf{v}'_b) + \omega_{cd}(\mathbf{v}'_c - \mathbf{v}'_d) - \nabla_c U_{abcd}(\mathbf{v}'_a, \ldots, \mathbf{v}'_d) &= \mathbf{o} \\
\omega_{ad}(\mathbf{v}'_d - \mathbf{v}'_a) + \omega_{bd}(\mathbf{v}'_d - \mathbf{v}'_b) + \omega_{cd}(\mathbf{v}'_d - \mathbf{v}'_c) - \nabla_d U_{abcd}(\mathbf{v}'_a, \ldots, \mathbf{v}'_d) &= \mathbf{o}
\end{aligned}
\tag{22}
$$

which is again overdetermined (12 equations in six unknowns $\omega_{ab}, \omega_{ac}, \omega_{ad}, \omega_{bc}, \omega_{bd}$ and ω_{cd}). Again direct computations show that there exists a unique solution if V'_a, V'_b, V'_c, V'_d span a 3-space; otherwise even a positive dimensional solution set exists. Thus one can substitute $\nabla_a U_{abcd}(\mathbf{v}'_a, \ldots, \mathbf{v}'_d)$ by a linear combination $\omega_{ab}(\mathbf{v}'_a - \mathbf{v}'_b) + \omega_{ac}(\mathbf{v}'_a - \mathbf{v}'_c) + \omega_{ad}(\mathbf{v}'_a - \mathbf{v}'_d)$ where the coefficients ω_{ab}, ω_{ac} and ω_{ad} are compatible with the other equations of (22).

Summing up the results of the three items shows that $\nabla_a u(\mathbf{V}')$ can be written in the form of Eq. (1) which proves the theorem for $\nu < 1/2$.

For $\nu = 1/2$ we have to compute the critical points of the Lagrange function

$$
F(\mathbf{V}', \lambda) = u(\mathbf{V}') - \lambda_1 f_1 - \ldots - \lambda_\varphi f_\varphi \quad \text{with} \quad \lambda := (\lambda_1, \ldots, \lambda_\varphi),
\tag{23}
$$

where $f_1, \ldots, f_\varphi$ are the isochoric constraints of the form $\mathrm{Vol}'^2_{abcd} - \mathrm{Vol}^2_{abcd} = 0$ for $abcd \in \mathscr{C}_j$ for all $j = p+1, \ldots, q$; i.e $\varphi = \sum_{j=p+1}^{q} \#\mathscr{C}_j$. Due to the Cayley-Menger determinant we get the squared volume V'^2_{abcd} of the tetrahedron spanned by $V'_a, \ldots, V'_d$, as a polynomial in the squared distances of these vertices. Now one can replace in Eq. (22) the function $U_{abcd}(\mathbf{v}'_a, \ldots, \mathbf{v}'_d)$ by $V'^2_{abcd}(\mathbf{v}'_a, \ldots, \mathbf{v}'_d)$ and do the analogous computation ending up with the same conclusion. Therefore $\nabla_a F(\mathbf{V}', \lambda)$ is again of the form of Eq. (1) which proves the theorem for $\nu = 1/2$. $\square$

Remark 4. *One can also ask for the critical points of the elastic strain energy density $u(\mathbf{L}')$; i.e. we have to consider the partial derivatives with respect to the edge lengths L'_{ij}. It can easily be seen that there is only one valid critical point namely $\mathbf{L}' = \mathbf{L}$ as all other solutions of the resulting system imply at least one edge of zero length. These invalid solutions can be avoided by considering $u(\mathbf{Q}')$ of Remark 2 and its partial derivatives with respect to Q'_{ij} ending up in a linear system.* ⬦

For the formulation of the next theorem we also need the notation of stability. A realization $G(\mathbf{V}')$ is called stable if it corresponds to a local minimum of the total elastic strain energy of the framework, which is also a minimum of the strain energy density $u(\mathbf{V}')$.

Theorem 2. *If a pin-jointed body-bar framework snaps out of a stable realization $G(\mathbf{V})$ by applying the minimum strain energy needed to it, then the corresponding deformation passes a realization $G(\mathbf{V}')$ at the maximum state of deformation, where the equivalent bar-joint framework $G_*(\mathbf{V}')$ has a non-zero self-stress.*

Proof: We think of u as a graph function over the space $\mathbb{R}^{wd}$ of knot configurations. In order to get out of the valley of the local minimum $(\mathbf{V}, u(\mathbf{V}))$, which corresponds to the given stable realization $G(\mathbf{V})$, with a minimum of energy needed, one has to pass a *saddle point* $(\mathbf{V}', u(\mathbf{V}'))$ of the graph, which corresponds to a realization $G(\mathbf{V}')$. As local extrema as well as saddle points of the graph function are given by the critical points of u we can use Theorem 1, which implies that these points correspond with self-stressed realizations of the equivalent bar-joint framework. As $u(\mathbf{V}') > 0$ holds the realization $G_*(\mathbf{V}')$ is deformed which has to imply a non-zero self-stress; i.e. the stress-vector ω differs from the b-dimensional zero vector. $\square$

---

[11]As a triangle is planar, we get in total 6 equations in three unknowns from Eq. (21).

Corollary 1. *If the equivalent bar-joint framework of Theorem 2 is minimally rigid, then "non-zero self-stress" can be replaced by "shakiness".*

Proof: If the equivalent bar-joint framework is minimally rigid then the existence of a non-zero self-stress implies a rank defect of the square rigidity matrix (cf. end of Section 1.2), which results in an infinitesimal flexibility. ☐

But also without the assumption of minimal rigidity used in Corollary 1, one can give the following connection between shakiness and snapping.

Theorem 3. *One can replace "non-zero self-stress" by "shakiness" in Theorem 2 if there exists a deformation such that the path from $G_*(\mathbf{V})$ to $G_*(\mathbf{V}')$ is identical to the path of $G_*(\mathbf{V}'')$ to $G_*(\mathbf{V}')$ in the space of intrinsic framework metrics $\mathbb{R}^b$, where $G_*(\mathbf{V})$ and $G_*(\mathbf{V}'')$ are not related by a direct isometry.*

Proof: Let us assume that there exists a path $(\mathbf{V}_t, u(\mathbf{V}_t))$ on the graph with parameter $t \in [0,1]$ such that for $t = 0$ we are at $(\mathbf{V}, u(\mathbf{V}))$ and for $t = 1$ at the saddle $(\mathbf{V}', u(\mathbf{V}'))$. This deformation implies a path $\mathbf{L}_t$ in the space $\mathbb{R}^b$ of intrinsic metrics with $\mathbf{L}_t\big|_{t=1} = \mathbf{L}'$ and $\mathbf{L}_t\big|_{t=0} = \mathbf{L}$.
But vice versa the path $\mathbf{L}_t$ corresponds to several 1-parametric deformations in $\mathbb{R}^d$, where one of these deformations $(\overline{\mathbf{V}}_t, u(\overline{\mathbf{V}}_t))$ has to lead towards $(\mathbf{V}'', u(\mathbf{V}''))$ according to our assumption. Moreover, tracking the realizations of the path $\mathbf{L}_t$ with $t \in [0,1]$ shows that in $G_*(\mathbf{V}')$ two realizations coincide, which implies that $G_*(\mathbf{V}')$ is shaky. ☐

Remark 5. *Note that $G(\mathbf{V}'')$ can also be a complex realization. In this case the deformation $(\overline{\mathbf{V}}_t, u(\overline{\mathbf{V}}_t))$ towards $(\mathbf{V}'', u(\mathbf{V}''))$ get stuck on the border of reality. Therefore the snap ends up in a realization of the equivalent bar-joint framework, which is shaky as a real solution of an algebraic set of equations can only change over into a complex one through a double root.* ◇

If the two realizations $G_*(\mathbf{V})$ and $G_*(\mathbf{V}'')$ of Theorem 3 are thought infinitesimal close to $G_*(\mathbf{V}')$ then we get the following characterization of shakiness:

Corollary 2. *$G_*(\mathbf{V}')$ is shaky, if three exist two instantaneous snapping deformations ($\neq$ infinitesimal isometric deformations) out of $G_*(\mathbf{V}')$ represented by two non-zero vectors in $\mathbb{R}^{wd}$ pointing into distinct directions, whose corresponding two vectors of instantaneous changes of the intrinsic metric in $\mathbb{R}^b$ are identical.*

Remark 6. *Note that within the set of pairs of vectors fulfilling Corollary 2, there exists at least one pair of oppositely directed vectors in $\mathbb{R}^{wd}$, which both correspond to the zero-vector in $\mathbb{R}^b$.* ◇

Based on Theorem 2 we can evaluate the snappability of the pin-jointed body-bar framework $G(\mathcal{K})$ in the undeformed realization $G(\mathbf{V})$ by the value $s(\mathbf{V}) := d(\mathbf{L}, \mathbf{L}') = u(\mathbf{L}')/E$, which we call *local snappability*. As in general a framework has several undeformed realizations $G(\mathbf{V}_1), \ldots, G(\mathbf{V}_k)$ we can define a *global snappability* by $s(\mathbf{L}) := \min\{s(\mathbf{V}_1), \ldots, s(\mathbf{V}_k)\}$.

4.1 Computation of the local snappability

We compute the critical points of the Lagrange function of Eq. (23) by using the homotopy continuation method (e.g. Bertini; cf. [40]) as other approaches (e.g. Gröbner base, resultant based elimination) are not promising due to the number of unknowns and degree of equations. By choosing a suitable reference frame we can reduce the number of unknowns by 6 for $d = 3$ and by 3 for $d = 2$, respectively, which also eliminates isometries (cf. footnote 3).

Remark 7. *The computation of the critical points, which depends heavily on the number of unknowns, can be a time consuming task in the first run of the homotopy. But if one changes the inner metric of the framework within the design process the critical points of the resulting new system of equations can be computed from the already known critical points of the initial system more efficiently by means of parameter homotopy [40].* ◇

First of all we can restrict to the obtained real critical points as only these correspond to realizations. This resulting set $\mathscr{R}$ of realizations is split into a set $\mathscr{E}$, whose elements correspond to local extrema of $u(\mathbf{V}')$, and its absolute complement $\mathscr{S} = \mathscr{R} \setminus \mathscr{E}$ of so-called *saddle realizations*. This separation can be done by the *second partial derivative test* based on the *Hessian matrix* of the function $u(\mathbf{V}')$ or in the case of side conditions one has to use the bordered Hessian [41] of the Lagrangian $F(\mathbf{V}', \lambda)$. Let us denote the set of stable realizations by $\mathscr{M} \subset \mathscr{E}$, which correspond to local minima.
One way for computing the local snappability is to start at saddle points and apply gradient descent algorithms to find neighboring local minima. This was done in the following example of a full quad.

Example 1. *We consider a full quad with vertices A, B, C, D. Its intrinsic metric is given by:*

$$\overline{AB} = 6, \quad \overline{CD} = \sqrt{8}, \quad \overline{AC} = \overline{BD} = \sqrt{17}, \quad \overline{AD} = \overline{BC} = \sqrt{5}. \tag{24}$$
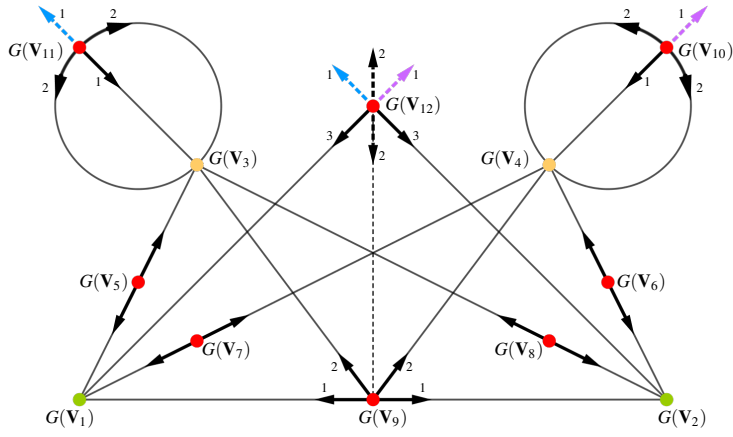
Fig. 1. Directed graph relating the stable realizations (undeformed green and deformed yellow) and saddle relations (red), where the orientation points towards local minima. The number i beside an arrow refers to the gradient flow in direction of the i-th smallest main curvature. If this number is missing, then there is only one negative main curvature direction. The two blue/violet dotted arrows indicate that these two flows end up in a realization obtained from $G(\mathbf{V}_{3/4})$ by reflecting it at the y-axis ($\Rightarrow x_1 < 0$ which contradicts our assumption). The edge and arrow between $G(\mathbf{V}_{12})$ and $G(\mathbf{V}_9)$ are dotted as under this gradient flow all points move along the x-axis, which imply that some edge lengths become zero during the deformation. But taking small perturbations into account these zeros can be avoided. As this arrow appears between two saddle realizations, it means that $G(\mathbf{V}_{12})$ can also be deformed into $G(\mathbf{V}_3)$ and $G(\mathbf{V}_4)$, respectively. The second black dotted arrow pointing upwards indicate that this flow ends up in the mirrored realization of $G(\mathbf{V}_9)$ ($\Rightarrow x_1 < 0$ which contradicts our assumption). Finally it should be noted that the transition between the undeformed realizations $G(\mathbf{V}_1)$ and $G(\mathbf{V}_2)$ can not only be done by snaps over the shaky realizations $G(\mathbf{V}_9)$ and $G(\mathbf{V}_{12})$, respectively, but also by two subsequent snaps from $G(\mathbf{V}_1)$ over $G(\mathbf{V}_{5/7})$ to $G(\mathbf{V}_{3/4})$ and further over $G(\mathbf{V}_{8/6})$ to $G(\mathbf{V}_2)$, without passing a shaky realization.

For the computation we coordinatize the vertices as follows:

$$A = (-x_1, 0), \quad B = (x_1, 0), \quad C = (x_2, y_2), \quad D = (x_3, y_3). \tag{25}$$

In this way the bar from A to B is attached to the x-axis of the reference frame. Due to the fact that a bar cannot have zero length, we restrict ourselves to realizations of $\mathcal{M}$ and $\mathcal{S}$ where no points coincide. Moreover, we can assume without loss of generality that $x_1 > 0$ holds, as a continuous deformation between a realization with $x_1 < 0$ and a realization with $x_1 > 0$ has to pass $x_1 = 0$ ($\Leftrightarrow A = B$). A in-depth analysis of the remaining critical points results in Fig. 1, which shows a directed graph relating the local minima and saddle points, where the orientation points towards local minima. The stable realizations are illustrated in Fig. 2 and the saddle realizations in Figs. 3 and 4, respectively. Representative snaps (transitions) between stable realizations are illustrated in Fig. 5.

Even though this framework is globally rigid we get two undeformed realizations $G(\mathbf{V}_1)$ and $G(\mathbf{V}_2)$, which are mirror-symmetric with respect to the x-axis (Fig. 2). Moreover, it is possible to snap from $G(\mathbf{V}_1)$ into $G(\mathbf{V}_2)$ (cf. Figs. 1 and 5). Thus the property of being globally rigid cannot save the framework from the snapping phenomenon.

The values for $u(\mathbf{V}_i)/E$ as well as x_1, x_2, y_2, x_3, y_3 of the stable/saddle realizations are given in Table 1. From these values and the graph given in Fig. 1 one sees that the two local snappabilities are equal; thus $s(\mathbf{L}) = s(\mathbf{V}_1) = s(\mathbf{V}_2) = 0.017411595327$ holds.

Fig. 2. Local minima: The two undeformed realizations $G(\mathbf{V}_1)$ and $G(\mathbf{V}_2)$ and the two deformed stable realizations $G(\mathbf{V}_3)$ and $G(\mathbf{V}_4)$ (from left to right). The point A is colored red, B green, C blue and D yellow, respectively. This color-coding is also used in the Figs. 3–5.

Fig. 3. Saddle points: These four realizations $G(\mathbf{V}_5), \ldots, G(\mathbf{V}_8)$ (from left to right) correspond to saddle points. Three points look to be collinear but they are not (cf. values given in Table 1).

Fig. 4. Saddle points: These four realizations $G(\mathbf{V}_9), \ldots, G(\mathbf{V}_{12})$ (from left to right) correspond to saddle points. Moreover, the realizations $G(\mathbf{V}_9)$ and $G(\mathbf{V}_{12})$ are shaky realizations.
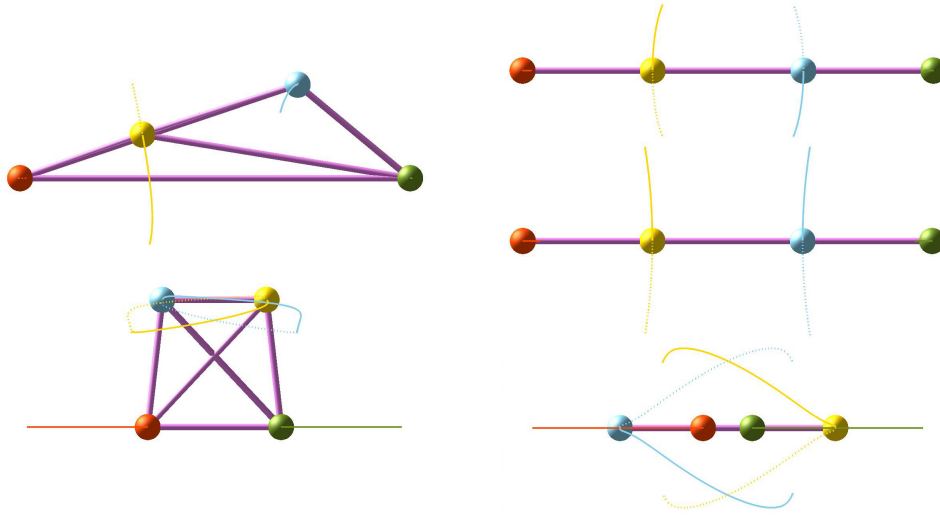

Fig. 5. The gradient flows starting at some saddle realizations in direction of negative main curvature. In one direction the paths of the points are plotted solid and in the opposite direction dotted. Upper left: Saddle realization $G(\mathbf{V}_5)$ and the corresponding paths of the points towards the realizations $G(\mathbf{V}_1)$ and $G(\mathbf{V}_3)$. Lower left: Following the gradient flow starting at the saddle realization $G(\mathbf{V}_{11})$ in direction of the second-smallest main curvature shows that both paths end up in the realization $G(\mathbf{V}_3)$. Therefore this realization can snap into itself over the saddle realization $G(\mathbf{V}_{11})$. Upper (center) right: Saddle realization $G(\mathbf{V}_9)$ and the gradient flow in direction of the smallest (second-smallest) main curvature. This shows the snapping between $G(\mathbf{V}_1)$ and $G(\mathbf{V}_2)$ ($G(\mathbf{V}_3)$ and $G(\mathbf{V}_4)$) over the shaky realization $G(\mathbf{V}_9)$. By combining the different gradient flows $G(\mathbf{V}_1)$ can also snap into $G(\mathbf{V}_3)$ over $G(\mathbf{V}_9)$, but one needs more deformation energy compared to the snap over the saddle realization $G(\mathbf{V}_5)$ illustrated in the upper left corner (cf. Table 1). Lower right: Saddle realization $G(\mathbf{V}_{12})$ and the gradient flow in direction of the third-smallest main curvature. This shows an alternative snapping between $G(\mathbf{V}_1)$ and $G(\mathbf{V}_2)$, which also needs more deformation energy as the one over $G(\mathbf{V}_{12})$ illustrated in the upper right corner (cf. Table 1). Finally note that the three snaps illustrated in the right column also demonstrate Theorem 3 and on the infinitesimal level Corollary 2.

In practice one starts with the saddle realization $G(\mathbf{V}_i)$ with the lowest value for $u(\mathbf{V}_i)/E$ and compute gradient flows towards the stable realizations, hoping that one ends up in the undeformed realization under consideration. If one does not find such a descent path, then one repeats the procedure for the saddle realization with the next higher value for $u(\mathbf{V}_i)/E$. The problem of this approach is that one has no guarantee to detected all local minima which can be reached from a saddle point by a descent path. With guarantee one can only give a lower bound[12] for the global snappability by the following value:

Lemma 3. *Let us assume that $G(\mathbf{V}^-) \in \mathscr{S}$ implies the minimal value for $d(\mathbf{L}, \mathbf{L}^-)$ for all elements of $\mathscr{S}$. As a result $o(\mathbf{L}) := d(\mathbf{L}, \mathbf{L}^-) \leq s(\mathbf{L})$ has to hold.* ◇

Therefore we want to present a more sophisticated approach, which allows us to check directly if a saddle realization and

---

[12] Note that $o(\mathbf{L})$ can be seen as a kind of separation bound [42] of the real roots of the polynomial $u(\mathbf{V}')$ in terms of the intrinsic metric of framework inducing this polynomial.

	x_1	x_2	y_2	x_3	y_3	$u(\mathbf{V}_i)/E$
$\mathbf{V}_1$	3	1	1	-1	-1	0
$\mathbf{V}_2$	3	1	-1	-1	1	0
$\mathbf{V}_3$	2.873803815106	1.264482434547	1.435718952668	-1.264482434547	1.435718952668	0.014510412969
$\mathbf{V}_4$	2.873803815106	1.264482434547	-1.435718952668	-1.264482434547	-1.435718952668	0.014510412969
$\mathbf{V}_5$	2.984971064849	1.262815500919	1.420716567414	-1.110499467187	0.662434022361	0.017411595327
$\mathbf{V}_6$	2.984971064849	1.262815500919	-1.420716567414	-1.110499467187	-0.662434022361	0.017411595327
$\mathbf{V}_7$	2.984971064849	1.110499467187	-0.662434022361	-1.262815500919	-1.420716567414	0.017411595327
$\mathbf{V}_8$	2.984971064849	1.110499467187	0.662434022361	-1.262815500919	1.420716567414	0.017411595327
$\mathbf{V}_9$	3.139661485127	1.152372944387	0	-1.152372944387	0	0.029190294037
$\mathbf{V}_{10}$	1.023109368578	-0.801485412727	-1.942382880068	0.801485412727	-1.942382880068	0.544598068230
$\mathbf{V}_{11}$	1.023109368578	-0.801485412727	1.942382880068	0.801485412727	1.942382880068	0.544598068230
$\mathbf{V}_{12}$	0.377904764722	-1.656968246848	0	1.656968246848	0	0.606663470611

Table 1.   Coordinates of stable/saddle realizations and their corresponding $u(\mathbf{V}_i)/E$ value.

a stable realization can be deformed continuously into each other, whereby the deformation energy density has to decrease monotonically. The minor drawback of this method is that it only works for pin-jointed body-bar framework, which are isostatic.

4.2 Pin-jointed body-bar frameworks with minimal rigidity under affine deformations

We assume that the given pin-jointed body-bar framework $G(\mathscr{K})$ is isostatic[13]. By replacing the bodies by the corresponding globally rigid subframeworks, the equivalent body-bar framework $G_*(\mathscr{K}_*)$ is also isostatic, if all polyhedra (polygonal panels) are tetrahedral (triangular). But in the general case the subframeworks are overbraced.

The edges of the overbraced subframeworks are involved in the computation of the density function given in Lemma 1. One can get rid of this property by allowing only affine (homogeneous) deformations of the bodies. In this way every polyhedron (polygonal panel) can be represented by a tetrahedron V_a, V_b, V_c, V_d (triangle V_a, V_b, V_c) and the remaining vertices of the deformed polyhedron (polygonal panel) can then be obtained by the affine transformation determined by $V_i \mapsto V_i'$ for $i \in \{a,b,c,d\}$ (resp. $i \in \{a,b,c\}$).

As a consequence we can consider a minimal set of lengths L_{ij} which contains the lengths of the bars $\in \mathscr{G}$ plus for each polyhedron (polygonal panel) we get six (three) additional lengths. We collect these lengths within the vectors $\widetilde{\mathbf{L}} := (\ldots, L_{ij}, \ldots)^T \in \mathbb{R}^a$ and $\widetilde{\mathbf{Q}} := (1, \ldots, Q_{ij}, \ldots)^T \in \mathbb{R}^{a+1}$ with $a \leq b$. Using this notation the density function can be rewritten as follows:

$$u(\widetilde{\mathbf{L}}') := \frac{\sum_{ab \in \mathscr{G}} U_{ab}(\widetilde{\mathbf{L}}') + \sum_{i=1}^{p} \mathrm{Vol}(B_i^2)\left[\frac{U_{abc}(\widetilde{\mathbf{L}}')}{\mathrm{Vol}_{abc}}\right] + \sum_{j=p+1}^{q} \mathrm{Vol}(B_j^3)\left[\frac{U_{abcd}(\widetilde{\mathbf{L}}')}{\mathrm{Vol}_{abcd}}\right]}{\sum_{ab \in \mathscr{G}} \mathrm{Vol}_{ab} + \sum_{i=1}^{p} \mathrm{Vol}(B_i^2) + \sum_{j=p+1}^{q} \mathrm{Vol}(B_j^3)} \tag{26}$$

for an arbitrary $abc \in \mathscr{C}_i$ and $abcd \in \mathscr{C}_j$, respectively. As we can replace L'_{ij} in $u(\widetilde{\mathbf{L}}')$ by $\|\mathbf{v}'_i - \mathbf{v}'_j\|$ the function u can be computed in dependence of $\widetilde{\mathbf{V}}' \in \mathbb{R}^{\tilde{w}d}$ with $\tilde{w} = r + 3p + 4(q-p)$, where $\widetilde{\mathbf{V}}'$ contains the vectors of the vertices $V_1, \ldots, V_r$ as well as three vertices of each polygonal panel and four vertices of each polyhedron, respectively. With respect to the resulting density function $u(\widetilde{\mathbf{V}}')$ we compute the set $\mathscr{M}$ of stable realizations and the set $\mathscr{S}$ of saddle realizations. Moreover, the following theorem holds true:

Theorem 4. *If an isostatic pin-jointed body-bar framework snaps out of a stable realization $G(\mathbf{V})$ by applying the minimum strain energy needed to it, then the framework passes a realization $G(\mathbf{V}')$ at the maximum state of deformation (under the assumption that each body is deformed affinely), which is either shaky or contains at least a body of reduced dimension.*

Proof: For the analysis of the equations $\nabla_a u(\widetilde{\mathbf{V}}') = 0$ we use the sum rule for derivatives to study each summand separately.

---

[13]Note that the isostaticity of a spatial framework is a problem for its own and not treated within this article (see e.g. [43,44])

Let us assume that the vertex $V_a \in B_i$ is a vertex of a tetrahedron (triangle) representing a polyhedron (polygonal panel). From Theorem 1 it is already known that $\nabla_a U_{abcd}(\mathbf{v}'_a, \mathbf{v}'_b, \mathbf{v}'_c, \mathbf{v}'_d)$ (resp. $\nabla_a U_{abc}(\mathbf{v}'_a, \mathbf{v}'_b, \mathbf{v}'_c)$) can be written as a linear combination of the involved vectors (cf. Eq. (21) and Eq. (22), respectively). Therefore we are only left with the partial derivative of the elastic strain energy of a bar $ex \in \mathcal{G}$ with $V_e \in B_i$, i.e.

$$\mathbf{v}_e = \mathbf{v}_a + \xi(\mathbf{v}_b - \mathbf{v}_a) + \upsilon(\mathbf{v}_c - \mathbf{v}_a) + \zeta(\mathbf{v}_d - \mathbf{v}_a) \tag{27}$$

where $\zeta = 0$ holds for a polygonal panel. We get:

$$\nabla_a U_{ex}(\mathbf{v}'_a, \mathbf{v}'_b, \mathbf{v}'_c, \mathbf{v}'_d, \mathbf{v}'_x) = \tfrac{\text{Area}_{ex}(L'^2_{ex} - L^2_{ex})}{2 L^3_{ex}} \left[\xi(\mathbf{v}'_b - \mathbf{v}'_a) + \upsilon(\mathbf{v}'_c - \mathbf{v}'_a) + \zeta(\mathbf{v}'_d - \mathbf{v}'_a) + \mathbf{v}'_a - \mathbf{v}'_x \right] (1 - \xi - \upsilon - \zeta). \tag{28}$$

This shows that $\nabla_a u(\widetilde{\mathbf{V}}')$ can be written as a linear combination of the partial derivatives of the squared distances of vertices linked by tetrahedral (triangular) edges or green edges (edges $\in \mathcal{G}$).

As a consequence, each solution of the $\tilde{w}$ equations of the form $\nabla_i u(\widetilde{\mathbf{V}}') = 0$ can be associated with a $\tilde{w}d$-dimensional stress-vector ω. If this vector differs from the zero vector then the solution has to imply a rank defect of the square matrix, whose columns are the gradient vectors of the realization equations $c_1, \ldots, c_{\tilde{w}d}$. This rank defect either corresponds with a shaky configuration of the framework $G(\mathbf{V}')$ or arises from the shakiness of a substructure (i.e. a tetrahedron or a triangle) substituting a body. A tetrahedron (triangle) can only become infinitesimal flexible if its dimension is reduced to at least a plane (line). $\square$

An advantage of Theorem 4 over Theorem 2 is that the property of the realization $G(\mathbf{V}')$ concerns the pin-jointed body-bar framework and not the equivalent bar-joint framework (assumed that the given pin-jointed body-bar framework is not a bar-joint framework).

Is the assumption of affine deformations really a restriction? For our preferred choice of $v = 1/2$ the volume has to be constant. This has the following consequences for the deformation of polyhedra and polygonal panels, respectively.

- Assume a polyhedron $B^3_j(n_j)$ with $n_j > 4$ is given. Moreover, we assume that (b,c,d,e), (a,c,d,e), (a,b,d,e) and (a,b,c,e) belong to the index set $\mathcal{C}_j$ of non-degenerated tetrahedra. Therefore one can compute the barycentric coordinates of V_e with respect to the tetrahedron $V_a, \ldots, V_d$, which equal the ratio of the oriented volumes $(\text{Vol}_{bcde} : \text{Vol}_{acde} : \text{Vol}_{abde} : \text{Vol}_{abce})$ according to [45].
  Now we assume that the tetrahedron $V_a, \ldots, V_d$ was deformed isochoricly into $V'_1, \ldots, V'_4$. Therefore not only the volume remains constant under the deformation, but also its orientation[14]. As a consequence the mapping from $V_1, \ldots, V_4$ to $V'_1, \ldots, V'_4$ can be written as

$$\mathbf{v}'_i = \mathbf{A}\mathbf{v}_i + \mathbf{a} \quad \text{with} \quad \det(\mathbf{A}) = 1 \quad \text{for} \quad i = a, b, c, d. \tag{29}$$

  Then V'_e is uniquely determined by its barycentric coordinates $(\text{Vol}'_{bcde} : \text{Vol}'_{acde} : \text{Vol}'_{abde} : \text{Vol}'_{abce})$ with respect to the tetrahedron $V'_a, \ldots, V'_d$ which have to equal the above given homogenous 4-tuple. This already implies that V'_e and V_e are also in the affine correspondence of Eq. (29) (e.g. [46, page 61]).
- Assume a polygonal panel $B^2_i(n_i)$ with $n_i > 3$ is given. Moreover, we assume that (b,c,d), (a,c,d) and (a,b,d) belong to the index set $\mathcal{C}_i$ of non-degenerated triangles. According to Section 3.2.2 the panel height h'_{abc} of the deformed triangular subpanel can be computed as $\text{Vol}_{abc}/\text{Area}'_{abc}$. According to the second item of Remark 2 this height can be identified with the height h'_i of the deformed panel. In order that the heights h'_{bcd}, h'_{acd} and h'_{abd} of the other three triangular subpanels are equal to h'_i the following ratio has to hold:

$$\text{Area}'_{abc} : \text{Area}'_{bcd} : \text{Area}'_{acd} : \text{Area}'_{abd} = \text{Area}_{abc} : \text{Area}_{bcd} : \text{Area}_{acd} : \text{Area}_{abd}. \tag{30}$$

  By means of planar barycentric coordinates it can be seen that all four points have to be mapped by an affine transformation:

$$\mathbf{v}'_i = \mathbf{A}\mathbf{v}_i + \mathbf{a} \quad \text{for} \quad i = a, b, c, d. \tag{31}$$

  Note that in this case the matrix $\mathbf{A}$ is not restricted to $\det(\mathbf{A}) = 1$ but one only has to assume that $\text{Area}'_{abc} \neq 0$. For $d = 2$ the condition $\text{Area}'_{abc} \neq 0$ is equivalent with $\det(\mathbf{A}) \neq 0$.

---

[14] A change in orientation can only happen in a flat pose of the tetrahedron, which has zero volume.

These considerations show that the assumption of affine deformations is no restriction in the case where the inner graph of the polyhedron (polygonal panel) is a complete graph on at most four (three) vertices. In the more general case of global rigidity, which is only known for $\mathbb{R}^2$ (and still open for $\mathbb{R}^3$; cf. Section 1.2) and characterized by 3-connectivity and redundant rigidity of the graph [31], this assumption is maybe[15] restrictive. Taking these possible minor restrictions into account, we can compute the local snappability in an efficient way as follows.

Algorithm for computing the local snappability. Given is an undeformed realization $G(\widetilde{\mathbf{V}}) \in \mathscr{M}$ and we want to determine $s(\widetilde{\mathbf{V}})$. To do so, we consider the saddle realization $G(\widetilde{\mathbf{V}}') \in \mathscr{S}$ which has the minimal value for $d(\widetilde{\mathbf{L}}, \widetilde{\mathbf{L}}')$ and define the transformation

$$\widetilde{\mathbf{Q}}_t := \widetilde{\mathbf{Q}} + t(\widetilde{\mathbf{Q}}' - \widetilde{\mathbf{Q}}) \quad \text{with} \quad t \in [0, 1]. \tag{32}$$

This gradient flow in the space of squared leg lengths (cf. Remark 4) implies a path $\widetilde{\mathbf{L}}_t$ in $\mathbb{R}^a$ between $\widetilde{\mathbf{L}}$ and $\widetilde{\mathbf{L}}'$. Along this path the deformation energy of each tetrahedron U_{abcd}, triangular panel U_{abc} as well as bar U_{ab} is *monotonic increasing* with respect to the path parameter t. This ensures that only the minimum mechanical work needed is applied on the framework to reach $G(\widetilde{\mathbf{V}}')$. This results from Lemma 1, as $U_{abcd}(\widetilde{\mathbf{L}}_t)$, $U_{abc}(\widetilde{\mathbf{L}}_t)$ as well as $U_{ab}(\widetilde{\mathbf{L}}_t)$ are quadratic functions in t, which are at their minima for $t = 0$. The path $\widetilde{\mathbf{L}}_t$ corresponds to different 1-parametric deformations of realizations in $\mathbb{R}^d$. If among these a deformation $G(\widetilde{\mathbf{V}}_t)$ with the property

$$G(\widetilde{\mathbf{V}}_t)\big|_{t=0} = G(\widetilde{\mathbf{V}}), \quad G(\widetilde{\mathbf{V}}_t)\big|_{t=1} = G(\widetilde{\mathbf{V}}') \tag{33}$$

exists, then the given realization $G(\widetilde{\mathbf{V}})$ is deformed into $G(\widetilde{\mathbf{V}}')$ under $\widetilde{\mathbf{L}}_t$. Computationally the property (33) can easily be checked as follows: We consider the set of algebraic *realization equations* $c_1, \ldots, c_n$ implied by the framework (cf. Section 1.2). Due to Eq. (32) the equations, which correspond to bar constraints, depend linearly on t. We have to track the path of the solution $\widetilde{\mathbf{V}}$ of this algebraic system while t is increasing from zero to one. This is a homotopy continuation problem which can be solved efficiently e.g. by the software Bertini [40, Section 2.3].

Remark 8. *Note that this approach has to be adapted in the special case that the undeformed realization $G(\widetilde{\mathbf{V}}) \in \mathscr{M}$ is shaky, as $\widetilde{\mathbf{V}}$ is a singular solution of the algebraic system for $t = 0$. In this case one has to solve the set of algebraic equations $c_1, \ldots, c_n$ for a random value $t_* \in (0, 1)$. The resulting solutions are then tracked by homotopy continuation back to the value $t = 0$. At least two paths have to lead down to $\widetilde{\mathbf{V}}$. The corresponding solutions at $t = t_*$ of these paths are then tracked by homotopy continuation up to the value $t = 1$ to check if one of them ends up at $\widetilde{\mathbf{V}}'$.* $\diamond$

If no deformation with the property (33) exists then we redefine $\mathscr{S}$ as $\mathscr{S} \setminus \left\{ G(\widetilde{\mathbf{V}}') \right\}$ and run again the procedure explained in this paragraph until we get the sought-after realization implying $s(\widetilde{\mathbf{V}})$. If we end up with $\mathscr{S} = \{\}$ then we set $s(\widetilde{\mathbf{V}}) = \infty$.

Remark 9. *Even if $G(\widetilde{\mathbf{V}})$ and $G(\widetilde{\mathbf{V}}')$ have the same volume, the deformation implied by Eq. (32) is in general not isochoric.* $\diamond$

5 Local and global singularity-distance

In the following we want to determine the real point $\mathbf{V}'''$ of the *shakiness variety* $V(J)$ (cf. end of Section 1.2) minimizing the value $d(\mathbf{L}, \mathbf{L}''')$, where $G(\mathbf{V})$ is the given undeformed realization of a pin-jointed body-bar framework $G(\mathscr{K})$. In addition there should again exist a 1-parametric deformation of $G(\mathbf{V})$ into $G(\mathbf{V}''')$ such that the deformation energy density has to increase monotonically. If this is the case we call $\varsigma(\mathbf{V}) = d(\mathbf{L}, \mathbf{L}''') = u(\mathbf{L}''')/E$ the *local singularity-distance*. By taking the minimum of all local singularity-distances of possible undeformed realizations of a framework we get the *global singularity-distance* $\varsigma(\mathbf{L})$; i.e. $\varsigma(\mathbf{L}) := \min \{\varsigma(\mathbf{V}_1), \ldots, \varsigma(\mathbf{V}_k)\}$.

In the general case one has to compute the local minima of the Lagrangian

$$F(\mathbf{V}', \lambda) = u(\mathbf{V}') - \lambda_1 f_1 - \ldots - \lambda_\varphi f_\varphi - \lambda_{\varphi+1} g_1 - \ldots - \lambda_{\varphi+\gamma} g_\gamma \quad \text{with} \quad \lambda := (\lambda_1, \ldots, \lambda_{\varphi+\gamma}), \tag{34}$$

where we recall that $g_1, \ldots, g_\gamma$ are the generators of the ideal J of the shakiness variety $A(J)$ and $f_1, \ldots, f_\varphi$ denote the side conditions for an isochoric deformation if this is desired. Starting from the corresponding realizations one can apply again

---

[15]To clarify this open problem, one has to study in more detail the properties of globally rigid inner graphs (cf. Definition 1).

gradient descent algorithms with respect to the function of the deformation energy density in order to find the neighboring stable realizations. Clearly, this strategy is faced with the same problems as already mentioned in Section 4.1. But for pin-jointed body-bar frameworks with minimal rigidity under affine transformations we are able to prove the following statements (Theorem 5 and Corollaries 3 and 4).

Theorem 5. *If the undeformed realization $G(\mathbf{V})$ is not shaky, then the local snappability $s(\mathbf{V})$ is a lower bound on the local singularity-distance $\varsigma(\mathbf{V})$; i.e. $s(\mathbf{V}) \leq \varsigma(\mathbf{V})$. If the realization $G(\mathbf{V}')$, which implies the snappability $s(\mathbf{V})$, is shaky, then the equality holds.*

Proof: We show the relation $s(\mathbf{V}) \leq \varsigma(\mathbf{V})$ indirectly by assuming $\varsigma(\mathbf{V}) < s(\mathbf{V})$. We denote the shaky realization implying $\varsigma(\mathbf{V})$ by $G(\mathbf{V}'')$ which corresponds to $\widetilde{\mathbf{L}}'' \in \mathbb{R}^a$. In analogy to Eq. (32) we consider the relation

$$\widetilde{\mathbf{Q}}_t := \widetilde{\mathbf{Q}} + t(\widetilde{\mathbf{Q}}'' - \widetilde{\mathbf{Q}}) \quad \text{with} \quad t \in [0,1] \tag{35}$$

defining a path $\widetilde{\mathbf{L}}_t$ in $\mathbb{R}^a$ between $\widetilde{\mathbf{L}}$ and $\widetilde{\mathbf{L}}''$, which corresponds to a set of 1-parametric deformations $\{G(\mathbf{V}_t^1), G(\mathbf{V}_t^2), \ldots\}$. A subset $\mathscr{D}$ of this set has the property $G(\mathbf{V}_t^i)|_{t=1} = G(\mathbf{V}'')$ where $\#\mathscr{D} > 1$ holds as $G(\mathbf{V}'')$ is shaky [2, 22]. Therefore the framework can snap out of $G(\mathbf{V})$ over $G(\mathbf{V}'')$ which contradicts $\varsigma(\mathbf{V}) < s(\mathbf{V})$ ($\Longrightarrow s(\mathbf{V}) \leq \varsigma(\mathbf{V})$). □

In the case of Theorem 5 the local snappability gives the radius of a guaranteed singularity-free sphere in the space of intrinsic framework metrics for a non-shaky realization. Note that in the space $\mathbb{R}^b$ of squared edge lengths Q_{ij} this singularity-free zone is bounded by a hyperellipsoid due to the third item of Remark 2.

Moreover, Theorem 5 implies the following statement:

Corollary 3. *If none of the undeformed realizations of a framework $G(\mathbf{V}_1), \ldots, G(\mathbf{V}_k)$ is shaky, then the global snappability $s(\mathbf{L})$ is a lower bound on the global singularity-distance $\varsigma(\mathbf{L})$.*

Note that in case of Corollary 3 also $o(\mathbf{L}) \leq \varsigma(\mathbf{L})$ has to hold due to Lemma 3. Therefore $\varsigma(\mathbf{L})$ as well as $o(\mathbf{L})$ are radii of guaranteed singularity-free spheres in the space of intrinsic framework metrics for any of the undeformed realizations.

Moreover, we can make the following statement on the reality of deformations:

Corollary 4. *The deformation associated with the local snappability $s(\mathbf{V}) = d(\mathbf{L}, \mathbf{L}')$, which is implied by Eq. (32), is guaranteed to be real, if not both realizations $G(\mathbf{V})$ and $G(\mathbf{V}')$ are shaky.*

Proof: A real solution of an algebraic set of equations can only change over into a complex one through a double root, which corresponds either to a (1) shaky realization or to a (2) body of reduced dimension. Case (1) is impossible due to Theorem 5. Moreover, case (2) can also not hold, which can be shown in the same way as in the proof of Theorem 5.

Therefore the entire path has to be real if at least one of the two realizations is not shaky. □

In the following example we want to demonstrate the results obtained so far.

Example 2. *We consider a closed serial chain composed of four directly congruent tetrahedral chain elements, which are jointed by four hinges. The studied example was given by Wunderlich [17] and is illustrated in Fig. 6. It has a threefold reflexion symmetry with respect to three copunctal lines, which are pairwise orthogonal. Using them as axes of a Cartesian frame, the vertices can be coordinatized as follows:*

$$A_1 = (u_1, v_1, w_1)^T \qquad A_2 = (-u_2, v_2, w_2)^T \qquad A_3 = (-u_1, -v_1, w_1)^T \qquad A_4 = (u_2, -v_2, w_2)^T \tag{36}$$
$$B_1 = (u_1, -v_1, -w_1)^T \qquad B_2 = (u_2, v_2, -w_2)^T \qquad B_3 = (-u_1, v_1, -w_1)^T \qquad B_4 = (-u_2, -v_2, -w_2)^T \tag{37}$$

The intrinsic metric of the framework is given by the following assignment:

$$
\begin{aligned}
\overline{A_1A_2} = \overline{A_2A_3} = \overline{A_3A_4} = \overline{A_4A_1} = \overline{B_1B_2} = \overline{B_2B_3} = \overline{B_3B_4} = \overline{B_4B_1} &= \tfrac{25\sqrt{3}-15}{(3\sqrt{2}+10)\sqrt{3}-3\sqrt{2}+6} \\[4pt]
\overline{A_1B_2} = \overline{A_2B_3} = \overline{A_3B_4} = \overline{A_4B_1} &= \tfrac{15+5\sqrt{3}}{(3\sqrt{2}+10)\sqrt{3}-3\sqrt{2}+6} \\[4pt]
\overline{A_1B_4} = \overline{A_2B_1} = \overline{A_3B_2} = \overline{A_4B_3} &= \tfrac{45-5\sqrt{3}}{(3\sqrt{2}+10)\sqrt{3}-3\sqrt{2}+6} \\[4pt]
\overline{A_1B_1} = \overline{A_2B_2} = \overline{A_3B_3} = \overline{A_4B_4} &= \tfrac{15\sqrt{2}(\sqrt{3}-1)}{(3\sqrt{3}-3)\sqrt{2}+10\sqrt{3}+6}
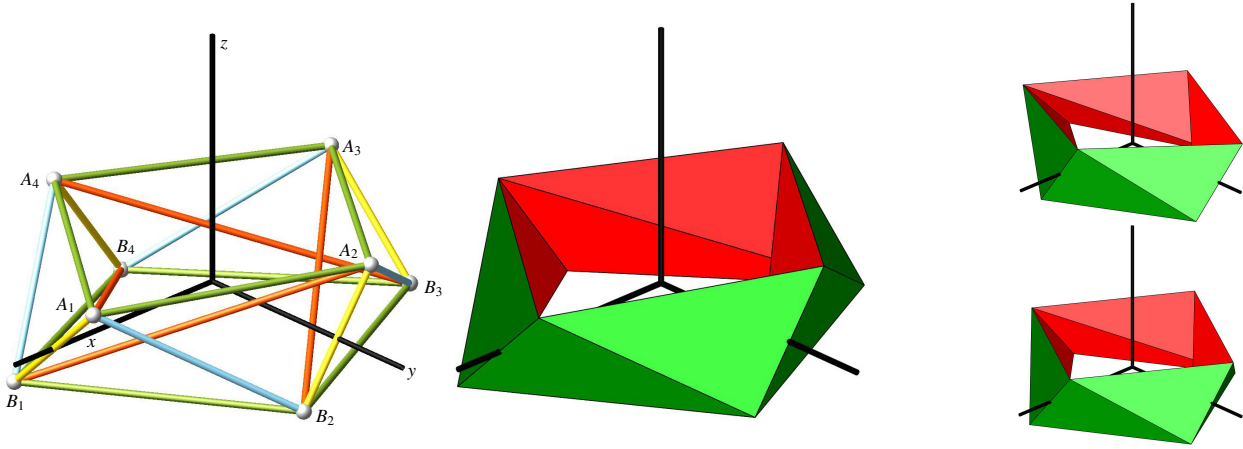\end{aligned} \tag{38}
$$

Fig. 6. Left: Illustration of the realization $G(\mathbf{V}_1)$ as a bar-joint framework, where bars of equal length have the same color. The four tetrahedra are hinged along the yellow bars. Moreover, the coordinate frame is displayed where the axes have a length of 1. Center: The same configuration as on the left side but illustrated with panels instead of bars. Congruent triangular panels are again same colored (either red or green). Right: At the top the second realization $G(\mathbf{V}_2)$ is visualized and at the bottom the shaky realization $G(\mathbf{V}')$. An animation of the snapping behavior can be downloaded from [47].

Chain elements		# tracked paths	#$\mathscr{R}$	#$\mathscr{S}$	$\varsigma(\mathbf{L}) = s(\mathbf{L})$
bar-joint		729	113	96	$6.762914466510 \cdot 10^{-7}$
panel-hinge	$\nu = 1/2$	729	161	144	$9.363722223978 \cdot 10^{-6}$
	$\nu = 1/4$	729	137	120	$1.052544771247 \cdot 10^{-5}$
	$\nu = 0$	729	129	112	$1.261816856140 \cdot 10^{-5}$
tetrahedra	$\nu = 1/2$	279 936	49	33	$3.289330211161 \cdot 10^{-5}$
	$\nu = 1/2$ (simple)	2 187	24	20	———— " ————
	$\nu = 1/4$	729	179	154	$3.946472039856 \cdot 10^{-5}$
	$\nu = 0$	729	178	155	$4.932700715589 \cdot 10^{-5}$

Table 2. Computational data: Note that the computation of the set $\mathscr{R}$ was done by a total degree homotopy using Bertini. For the case of tetrahedral chain elements under the assumption $\nu = 1/2$, the set $\mathscr{S}$ has to be filtered out from $\mathscr{R}$ by using a second-derivative test based on the bordered Hessian [41] due to the isochoricity side condition.

which has the property that the average edge length equals 1. We consider the two undeformed realizations $G(\mathbf{V}_1)$ and $G(\mathbf{V}_2)$ of the chain illustrated in Fig. 6, which can be computed according to the procedure given in [17]. The vector $(u_1, v_1, w_1, u_2, v_2, w_2)$ which corresponds to $\mathbf{V}_1$ is given by:

$$(0.802729630788, 0.207761716516, 0.207761716516, 0.169636731183, 0.655425998948, 0.239902565915) \quad (39)$$

The coordinates of $\mathbf{V}_2$ are obtained by the following exchange of the coordinate entries of $\mathbf{V}_1$: $u_1 \leftrightarrow v_2$, $v_1 \leftrightarrow u_2$ and $w_1 \leftrightarrow w_2$. Note that the framework can snap between the two realizations $G(\mathbf{V}_1)$ and $G(\mathbf{V}_2)$. The shaky saddle realization, which has to be passed during the snap, is denoted by $G(\mathbf{V}')$.

In general a closed chain composed of four tetrahedra results in an overbraced bar-joint framework, as one can remove e.g. the bars A_1B_4 and B_1B_4 to get a minimal rigid structure. But under the assumed threefold symmetry resulting in directly congruent chain elements the framework is minimal rigid, as the input of the six edge lengths $\overline{A_1B_1}$, $\overline{A_1B_2}$, $\overline{A_1A_2}$, $\overline{A_2B_1}$, $\overline{A_2B_2}$ and $\overline{B_1B_2}$ already determine the six values $u_1, u_2, v_1, v_2, w_1, w_2$ coordinatizing the four involved points and therefore the complete structure.

We can interpret the chain elements as bar-joint frameworks, panel-hinge frameworks or as tetrahedra. Moreover, in the case of triangular panels and tetrahedra we compute the snappability with respect to three different Poisson ratios $\nu = 0, \frac{1}{4}, \frac{1}{2}$. The computational data for the different cases is summarized in the Tables 2 and 3. Note that independent of the interpretation we get $s(\mathbf{L}) = s(\mathbf{V}_1) = s(\mathbf{V}_2)$. The corresponding saddle realizations $G(\mathbf{V}') \in \mathscr{S}$ (cf. Table 3) are all shaky

Chain elements		u_1, v_2	v_1, u_2	w_1, w_2
bar-joint		0.733113570223	0.186762548180	0.226463240099
panel-hinge	$v = 1/2$	0.733944401620	0.187601517133	0.226592028651
	$v = 1/4$	0.733918350832	0.187397874243	0.226701242326
	$v = 0$	0.733898439861	0.187273478928	0.226766038698
tetrahedra	$v = 1/2$	0.735389875237	0.190335899873	0.225439236330
	$v = 1/4$	0.735346467296	0.190324665294	0.225425929220
	$v = 0$	0.735317448771	0.190317154629	0.225417033375

Table 3. Coordinates of the shaky saddle realization $G(\mathbf{V}') \in \mathscr{S}$ for the different interpretations of the tetrahedra.
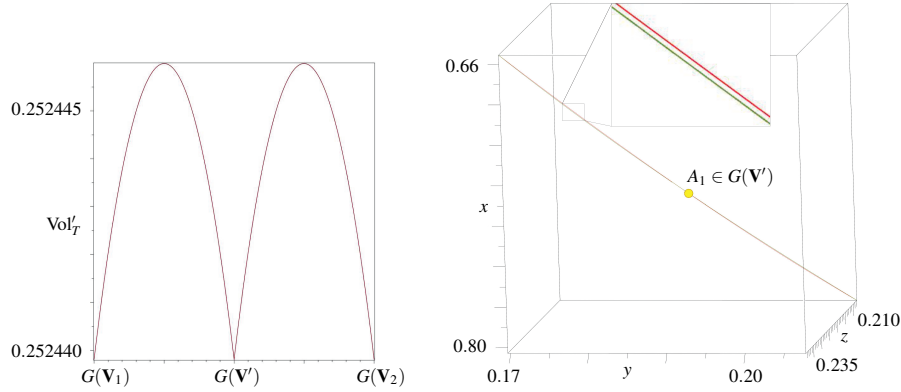
Fig. 7. Left: The change of the volume of a tetrahedron under the transformation implied by the gradient flow in the space of squared leg lengths (cf. Eq. (32) and Remark 9). The corresponding trajectory of the point A_1 is illustrated by the red curve in the right figure. The green curve corresponds to an isochoric deformation, which was computed with a projected gradient algorithm.

as they fulfill the equation $u_1 v_1 w_2 - u_2 v_2 w_1 = 0$ indicating that the Plücker coordinates of the four lines $A_i B_i$ are linearly dependent (cf. [48]). Note that for the interpretation as bar-joint framework or panel-hinge framework the singularity condition consists of a second factor $u_1 v_1 w_2 + u_2 v_2 w_1 = 0$ which implies the coplanarity of the vertices $A_i, B_i, A_{i+1}, B_{i+1}$ (mod 4) for $i = 1, \dots, 4$. According to Theorem 5 we get $s(\mathbf{L}) = s(\mathbf{V}_1) = s(\mathbf{V}_2) = \varsigma(\mathbf{V}_1) = \varsigma(\mathbf{V}_2) = \varsigma(\mathbf{L})$.

Concerning the interpretation of the chain as bar-joint framework we can give the maximal absolute and relative variation of a bar in length during the deformation which equals 0.002359150067 and 0.001715578691, respectively. Moreover, each edge must change its length in average absolutely by 0.001064975188 and relatively by 0.000993544934.

Remark 10. *In the case of interpreting the chain elements as panel-hinge frameworks or as tetrahedra, we also put v as a unknown in the optimization process as stated in Remark 3. Computing the critical points with Bertini resulted in $24\,576$ paths. For panel-hinge frameworks none of the local extrema for $0 \leq v < 1/2$ has a value less than $9.363722223978 \cdot 10^{-6}$ and for tetrahedra no local extrema exists within this interval. Thus in both cases we get the local minimum at the boundary $v = 1/2$.* ◇

We close this example with some remarks on the case, where the chain is assembled by four tetrahedra of Poisson ratio $v = 1/2$: Due to the symmetry of the chain we only have to consider one isochoric constraint $Vol_T'^2 - Vol_T^2 = 0$, where T stands for one of the tetrahedra with vertices $A_i, B_i, A_{i+1}, B_{i+1}$ (mod 4) for $i = 1, \dots, 4$. The computation of critical points of $u(\mathbf{V})$ under this constraint (cf. Eq. (34)) results in the tracking of $279\,936$ paths (cf. Table 2). If we also invest the information, that the orientation of the tetrahedra has to remain constant under an isochoric deformation (cf. footnote 14), we can use the simplified condition $Vol_T' - Vol_T = 0$ of oriented volumes, which has the half degree. This approach reduces the number of paths to $2\,187$ for the computation of $G(\mathbf{V}')$ given in Table 3. But we are still lacking for an efficient determination of an isochoric deformation from $G(\mathbf{V})$ into $G(\mathbf{V}')$ with a monotonically increasing deformation energy density. Until now we can only achieve such a deformation by a projected gradient descent approach resulting in Fig. 7.

Further demonstration/verification of our method is done in Appendix A, where two snapping model flexors are studied. Moreover, the obtained results are compared with those reported in the literature.

6 Singularity-distance computation for Stewart-Gough manipulators

A Stewart-Gough (SG) manipulator is a parallel robot consisting of a moving platform, which is connected over six telescopic legs to the base. These legs are anchored by spherical joints to the platform and the base (cf. Fig. 8). If the prismatic joints of the legs are fixed, then the pin-jointed body-bar framework is in general rigid. It is well-known, that it has an infinitesimal flexibility if and only if the carrier lines of the six legs belong to a linear line complex [49].

A detailed literature review on works dealing with the determination of the closest singular configuration to a given non-singular one, which is of interest for singularity-free path-planning and performance optimization of the robot, was done by the author in [50]. Most of these approaches (also the one presented in [50]) evaluate the closeness extrinsically (i.e. in the 6 dimensional configuration space) and not intrinsically (i.e. in the 6 dimensional space of prismatic joints). Up to the knowledge of the author only one work of Zein et al. [51] determines a singularity-free cube in the joint space of a 3-RPR manipulator, which is the planar analogue of a SG platform. For a detailed comparison of extrinsic and intrinsic singularity distance measures for planar 3-RPR manipulators we refer to [52].

In the following we want to compute the singularity-distance within the 6-dimensional joint space of the manipulator. As a SG manipulator is an isostatic body-bar framework, this computation can be based on Theorem 4 under the additional condition that the affine deformations of the platform and the base are restricted to direct isometries. In this case the function of the strain energy density of a SG manipulator simplifies to:

$$u(\mathbf{L}') = \frac{1}{\sum_{i=1}^{6} L_i} \sum_{i=1}^{6} \frac{(L_i'^2 - L_i^2)^2}{8L_i^3} \qquad (40)$$

where L_i (resp. L_i') denotes the length of the undeformed (resp. deformed) ith leg spanned by the platform anchor point V_i and the corresponding base anchor point V_{i+6}. The base can be pinned down[16], i.e. $\mathbf{v}_i' = \mathbf{v}_i$ for $i = 7, \ldots, 12$, and for the platform we set up an affine moving frame with origin V_1 and the three vectors $\mathbf{v}_2 - \mathbf{v}_1$, $\mathbf{v}_3 - \mathbf{v}_1$ and $(\mathbf{v}_2 - \mathbf{v}_1) \times (\mathbf{v}_3 - \mathbf{v}_1)$ under the assumption that V_1, V_2, V_3 are not collinear. Then one can compute the affine coordinates $(\xi_j, \upsilon_j, \zeta_j)$ of the points V_j with respect to this frame for $j = 4, 5, 6$, which can be used for writting down the coordinate vector of V_j' as follows:

$$\mathbf{v}_j' = \mathbf{v}_1' + \xi_j(\mathbf{v}_2' - \mathbf{v}_1') + \upsilon_j(\mathbf{v}_3' - \mathbf{v}_1') + \zeta_j[(\mathbf{v}_2' - \mathbf{v}_1') \times (\mathbf{v}_3' - \mathbf{v}_1')]. \qquad (41)$$

This affine transformation is an orientation preserving isometry if the three side conditions $e_i = 0$ with

$$e_1 := \|\mathbf{v}_2' - \mathbf{v}_3'\|^2 - \|\mathbf{v}_2 - \mathbf{v}_3\|^2, \quad e_2 := \|\mathbf{v}_3' - \mathbf{v}_1'\|^2 - \|\mathbf{v}_3 - \mathbf{v}_1\|^2 \quad \text{and} \quad e_3 := \|\mathbf{v}_1' - \mathbf{v}_2'\|^2 - \|\mathbf{v}_1 - \mathbf{v}_2\|^2 \qquad (42)$$

hold true. Under consideration of Eq. (41) one can write Eq. (40) in dependence of $\mathbf{v}_1', \mathbf{v}_2', \mathbf{v}_3'$, which is part of the Lagrangian

$$F(\mathbf{v}_1', \mathbf{v}_2', \mathbf{v}_3', \eta_1, \eta_2, \eta_3) = u(\mathbf{v}_1', \mathbf{v}_2', \mathbf{v}_3') - \eta_1 e_1 - \eta_2 e_2 - \eta_3 e_3. \qquad (43)$$

Remark 11. *By using the linear combination given in Eq. (41) instead of the formulation of Eq. (27) the number of side conditions forcing an isometric transformation is reduced from 6 to 3; i.e. $e_1 = e_2 = e_3 = 0$. In addition this formulation already restricts to direct isometries. Clearly, one can also use a parametrization of the Euclidean motion group (e.g. Study parameters) for the representation of $\mathbf{v}_1', \ldots, \mathbf{v}_6'$. We use here this so-called point-based formulation as it turned out to have certain computational advantages (cf. [53]).* ◇

The formulation given in Eq. (40) rely on the change of the leg lengths relative to its initial length. As we are now working in the joint space of the SG manipulator also the following function of absolute changes in the leg lengths makes sense:

$$l(\mathbf{L}') = \sum_{i=1}^{6} (L_i'^2 - L_i^2)^2. \qquad (44)$$

Therefore one can also substitute $u(\mathbf{v}_1', \mathbf{v}_2', \mathbf{v}_3')$ by $l(\mathbf{v}_1', \mathbf{v}_2', \mathbf{v}_3')$ in Eq. (43). For both Lagrangians, analogous considerations as done in the proof of Theorem 4 show that the saddle realizations have to be shaky (as the bodies cannot reduce in dimension due to the enforced direct isometries). We demonstrate this in the following example.

---

[16]In this context it should be mentioned that the results of the paper also hold for pinned frameworks (cf. [11, Section 3.3]).
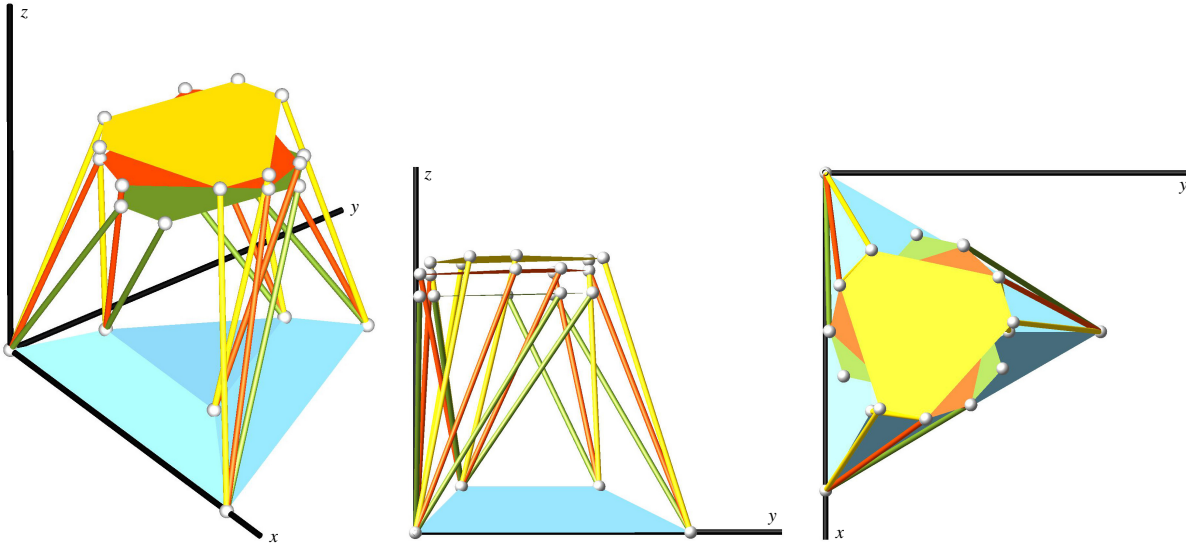
Fig. 8. Axonometric view (left), front view (center) and top view (right): $G(\mathbf{V}_1)$ is illustrated in yellow, $G(\mathbf{V}_2)$ is displayed in green and $G(\mathbf{V}')$ w.r.t. $u(\mathbf{L}')$ is shown in red. Note that the realization $G(\mathbf{V}')$ w.r.t. $l(\mathbf{L}')$ is not shown here as it is too close (cf. Table 5) to $G(\mathbf{V}')$ w.r.t. $u(\mathbf{L}')$.

Example 3. *We study a SG manipulator, which is of interest for practical applications, as the positioning and orientation of the relative pose of the platform and the base is decoupled (cf. [54, Section VI]). The moving platform has a semihexagonal shape (with central angles of $\pi/6$ and $\pi/2$, respectively) and the base is a truncated triangular pyramid (cf. Fig. 8). The coordinates of the base anchor points $V_7, \ldots, V_{12}$ with respect to the fixed frame are given by:*

$$\mathbf{v}_7 := \begin{pmatrix} 0 \\ 0 \\ 0 \end{pmatrix}, \quad \mathbf{v}_8 := \begin{pmatrix} \frac{\sqrt{3}}{2} \\ \frac{1}{2} \\ \frac{1}{2} \end{pmatrix}, \quad \mathbf{v}_9 := \begin{pmatrix} 2\sqrt{3} \\ 0 \\ 0 \end{pmatrix}, \quad \mathbf{v}_{10} := \begin{pmatrix} \frac{3\sqrt{3}}{2} \\ \frac{1}{2} \\ \frac{1}{2} \end{pmatrix}, \quad \mathbf{v}_{11} := \begin{pmatrix} \sqrt{3} \\ 3 \\ 0 \end{pmatrix}, \quad \mathbf{v}_{12} := \begin{pmatrix} \sqrt{3} \\ 2 \\ \frac{1}{2} \end{pmatrix}. \tag{45}$$

The vertices $V_1, \ldots, V_6$ of the moving platform are determined by the three conditions

$$\|\mathbf{v}_2 - \mathbf{v}_3\|^2 = 2, \quad \|\mathbf{v}_3 - \mathbf{v}_1\|^2 = 3, \quad \|\mathbf{v}_1 - \mathbf{v}_2\|^2 = 2 - \sqrt{3} \tag{46}$$

and the affine coordinates $(\xi_j, \upsilon_j, 0)$ for $j = 4, 5, 6$ given by

$$\xi_4 := -\frac{\sqrt{3}+1}{2}, \quad \upsilon_4 := \frac{\sqrt{3}+1}{2}, \quad \xi_5 := -\frac{3(\sqrt{3}+1)}{2}, \quad \upsilon_5 := \frac{\sqrt{3}+1}{2}, \quad \xi_6 := -\sqrt{3} - 2, \quad \upsilon_6 := 1. \tag{47}$$

The input data is completed by the following six leg lengths:

$$L_1 := 31/10, \quad L_2 := 25/10, \quad L_3 := 32/10, \quad L_4 := 26/10, \quad L_5 := 315/100, \quad L_6 := 255/100. \tag{48}$$

We compute the closest singularity with respect to both intrinsic metrics in the 6-dimensional joint space, which are given in Eq. (40) and Eq. (44), respectively. The computational data is summarized in Table 4.

For this input data the SG manipulator has 4 real solutions for the direct kinematics, whereby two solutions are out of interest as the platform is below the base. The other two undeformed realizations are illustrated in Fig. 8 and the corresponding vectors $\mathbf{v}_i = (x_i, y_i, z_i)^T$ (with respect to the fixed frame) of the platform anchor points V_i for $i = 1, 2, 3$ are given in Table 5. This table also contains the corresponding coordinate entries of the two saddle realization $G(\mathbf{V}')$, which imply the singularity-distance with respect to the different metrics. It can easily be checked that in both realizations $G(\mathbf{V}')$ the lines of the six legs belong to a linear line complex [49].

Remark 12. *Note that the snapping octahedra of Wunderlich [16] imply further examples of octahedral hexapods with a high snapping capability.* ◇

Intrinsic metric	# tracked paths	$\#\mathscr{R}$	$\#\mathscr{S}$	$\varsigma(\mathbf{L}) = s(\mathbf{L})$
$u(\mathbf{L}')$	26017	124	111	$3.324106490339 \cdot 10^{-5}$
$l(\mathbf{L}')$	25473	122	112	$1.024890249080 \cdot 10^{-1}$

Table 4. Computational data: Note that the computation of the set $\mathscr{R}$ was done by a regeneration homotopy performed with Bertini. Note that the set $\mathscr{S}$ has to be filtered out from $\mathscr{R}$ by using a second-derivative test based on the bordered Hessian [41] due to the three side conditions $e_1 = e_2 = e_3 = 0$.

	$\mathbf{V}_1$	$\mathbf{V}_2$	$\mathbf{V}'$ w.r.t. $u(\mathbf{L}')$	$\mathbf{V}'$ w.r.t. $l(\mathbf{L}')$
x_1	0.842928302224	1.722185861193	1.225741950663	1.221043138727
x_2	1.227117667465	2.215337180628	1.731161637163	1.726370305617
x_3	2.571092053711	2.516815584869	2.684588070901	2.680372134138
y_1	0.505604311407	0.043791592870	0.160342690355	0.156045184954
y_2	0.158839883661	0.201000858188	0.048866028718	0.044256807218
y_3	0.594205901934	1.582339155201	1.092093613851	1.086968370169
z_1	2.940040162536	2.577238474600	2.814950790353	2.824067090458
z_2	2.950147373651	2.583256403538	2.823499874485	2.833916224311
z_3	3.014872015394	2.615119877650	2.875019201615	2.885230039892

Table 5. Coordinates of the undeformed realizations $G(\mathbf{V}_1)$ and $G(\mathbf{V}_2)$ of the SG manipulator and of the shaky saddle realization $G(\mathbf{V}')$ with respect to both intrinsic metrics given in Eq. (40) and Eq. (44), respectively.

7 Conclusion

The first considerations in the design process of a pin-jointed body-bar framework concern its geometry. In this paper we presented an index, which evaluates the framework geometry with respect to its capability to snap. As this so-called *snappability* only depends on the intrinsic framework geometry, it enables a fair comparison of frameworks differing in the combinatorial structure, inner metric and types of structural elements (bars, polygonal panels or polyhedral bodies). Therefore it can serve engineers as a criterion in an early design stage for the geometric layout of frameworks without or with the capability to snap, depending on the application. In the context of multistability the index can for example be used for the geometric layouting of unit-cells/building-blocks of periodic metamaterials (e.g. [7, 8, 9, 29, 30]) and origami structures (e.g. hypar tessellation [6], waterbomb cylinder tessellation [5] or the Kresling pattern with a circular arrangement to closed strips, which correspond to snapping antiprisms [18] and can be composed to cylindrical towers [4, 55, 56], or a helical arrangement according to C.R. Calladine studied in [28, 57, 58, 59]). For the resulting framework geometry one can specify in a later design phase the material and dimensioning (e.g. profile of bars) of the framework elements in such a way that the wanted effects are even increased.

We also demonstrated on basis of parallel manipulators of Stewart-Gough type, that our approach can be used for the computation of intrinsic singular-distances. The computational aspects of the index were also illuminated and an allover algorithm was presented for isostatic frameworks (under affine deformation of the bodies). Note that this algorithm does not take the bending of panels into account and also ignores the collision of bars and/or bodies during the deformation. For overbraced frameworks we gave a strategy for the snappability computation but the result is without guarantee. In this case one can use the proposed lower bounds, which always hold true.

References

[1] Kiraly, C., Tanigawa, S.: Rigidity of Body-Bar-Hinge Frameworks. Handbook of Geometric Constraint Systems Principles (M. Sitharam et al. eds.), pages 435–459, CRC Press (2019)

[2] Wohlhart, K.: Degrees of shakiness. Mechanism and Machine Theory **34**(7) 1103–1126 (1999)

[3] Stachel, H.: What lies between rigidity and flexibility of structures. Serbian Architectural Journal **3**(2) 102–115 (2011)

[4] Liu, K., Paulino, G.H.: Nonlinear mechanics of non-rigid origami: an efficient computational approach. Proceedings of the Royal Society A **473**(2206) 2017.0348 (2017)

[5] Gillman, A, Fuchi, K., Buskohl, P.R.: Truss-based nonlinear mechanical analysis for origami structures exhibiting bifurcation and limit point instabilities. International Journal of Solids and Structures **147** 80–93 (2018)

[6] Liu, K., Tachi, T., Paulino, G.H.: Invariant and smooth limit of discrete geometry folded from bistable origami leading to multistable metasurfaces. Nature Communications **10** 4238 (2019)

[7] Haghpanah, B., Salari-Sharif, L., Pourrajab, P., Hopkins, J., Valdevit, L.: Multistable Shape-Reconfigurable Architected Materials. Advanced Materials **28**(36) 7915–7920 (2016)

[8] Shang, X., Liu, L., Rafsanjani, A., Pasini, D.: Durable bistable auxetics made of rigid solids. Journal of Materials Research **33**(3) 300–308 (2018)

[9] Yang, H., Ma, L.: 1D and 2D snapping mechanical metamaterials with cylindrical topology. International Journal of Solids and Structures **204–205** 220–232 (2020)

[10] Karpov, E.G., Ozevin, D., Mahamid, M., Danso, L.A.: On the comprehensive stability analysis of axially loaded bistable and tristable metastructures. International Journal of Solids and Structures **199** 158–168 (2020)

[11] Nawratil, G.: Evaluating the snappability of bar-joint frameworks. Advances in Robot Kinematics 2020 (J. Lenarcic, B. Siciliano eds.), pages 182–189, Springer (2020), arXiv:1910.04810

[12] Nawratil, G.: On the snappability and singularity-distance of frameworks with bars and triangular plates. In Springer's Proceedings in Advanced Robotics of the 2nd IMA Conference on Mathematics of Robotics (accepted), arXiv:2003.09904

[13] Schulze, B., Whiteley, W.: Rigidity and scene analysis. Handbook of Discrete and Computational Geometry (J.E. Goodman et al. eds.), pages 1593–1632, 3rd edition, CRC Press (2017)

[14] Izmestiev, I.: Statics and kinematics of frameworks in Euclidean and non-Euclidean geometry. Eighteen Essays in Non-Euclidean Geometry (V. Alberge, A. Papadopoulos eds.), pages 191–233, EMS Publishing House (2019)

[15] Stachel, H.: Configuration theorems on bipartite frameworks. Rendiconti del Circolo Matematico di Palermo (Series 2) **70**(II) 335–351 (2002)

[16] Wunderlich, W.: Starre, kippende, wackelige und bewegliche Achtflache. Elemente der Mathematik **20**(2) 25–32 (1965)

[17] Wunderlich, W.: Starre, kippende, wackelige und bewegliche Gelenksvierecke im Raum. Elemente der Mathematik **26**(4) 73–83 (1971)

[18] Wunderlich, W.: Snapping and Shaky Antiprisms. Mathematics Magazine **52**(4) 235–236 (1979)

[19] Wunderlich, W.: Kipp-Ikosaeder I. Elemente der Mathematik **36**(6) 153–158 (1981)

[20] Wunderlich, W.: Kipp-Ikosaeder II. Elemente der Mathematik **37**(3) 84–89 (1982)

[21] Wunderlich, W.: Wackeldodekaeder. Elemente der Mathematik **37**(6) 153–163 (1982)

[22] Stachel, H.: W. Wunderlichs Beiträge zur Wackeligkeit. Technical Report No. 22, Institute of Geometry, TU Wien (1995)

[23] Goldberg, M.: Unstable Polyhedral Structures. Mathematics Magazine **51**(3) 165–170 (1978)

[24] Milka, A.D.: Linear bendings of right convex polyhedra. Matematicheskaya fizika, anliz, geometriya **1**(1) 116–130 (1994)

[25] Wunderlich, W., Schwabe, C.: Eine Familie von geschlossenen gleichflächigen Polyedern, die fast beweglich sind. Elemente der Mathematik **41**(4) 88–93 (1986)

[26] Gorkavyy, V., Fesenko, I.: On the model flexibility of Siamese dipyramids. Journal of Geometry **110**:7 (2019)

[27] Holmes-Cerfon, M., Theran, L., Gortler S.J.: Almost-rigidity of frameworks. Communications on Pure and Applied Mathematics (to appear) arXiv:1908.03802

[28] Guest, S.D., Pellegrino, S.: The folding of triangulated cylinders, Part II: The folding process. Journal of Applied Mechanics **61**(4) 778–783 (1994)

[29] Danso, L.A., Karpov, E.G.: Cusp singularity-based bistability criterion for geometrically nonlinear structures. Extreme Mechanics Letters **13** 135–140 (2017)

[30] Klein, J.T., Karpov, E.G.: Bistability in thermomechanical metamaterials structured as three-dimensional composite tetrahedra. Extreme Mechanics Letters **29** 100459 (2019)

[31] Jackson, B., Jordan, T.: Connected rigidity matroids and unique realizations of graphs. Journal of Combinatorial Theory Series B **94**(1) 1–29 (2005)

[32] Asimow, L., Roth, B.: The Rigidity of Graphs. Transaction of the American Mathematical Society **245** 279–289 (1978)

[33] Connelly, R.: Rigidity. Handbook of Convex Geometry (P.M. Gruber, J.M. Wills eds.), pages 223–271, Elsevier (1993)

[34] Laman, G.: On graphs and rigidity of plane skeletal structures. Journal of Engineering Mathematics **4**(4) 331–340 (1970)

[35] Fedorchuk, M., Pak, I.: Rigidity and polynomial invariants of convex polytopes. Duke Mathematical Journal **129**(2) 371–404 (2005)

[36] White, N.L., Whiteley, W.: The algebraic geometry of stresses in frameworks. Siam Journal on Algebraic and Discrete

Methods **4**(4) 481–511 (1983)

[37] Logan, D.L.: A First Course in the Finite Element Method. 4th Ed., Thomson (2007)

[38] Reddy, J.N.: An Introduction to Nonlinear Finite Element Analysis. 2nd edition, Oxford University Press (2015)

[39] Reznick, B.: Some concrete aspects of Hilbert's 17th Problem. Real Algebraic Geometry and Ordered Structures (C.N. Delzell, J.J. Madden eds.), pages 251–272, AMS (2000)

[40] Bates, D.J., Hauenstein J.D., Sommese, A.J., Wampler C.W.: Numerically Solving Polynomial Systems with Bertini. SIAM Philadelphia (2013)

[41] Spring, D.: On the Second Derivative Test for Constrained Local Extrema. The American Mathematical Monthly **92**(9) 631–643 (1985)

[42] Herman, A., Hong, H., Tsigaridas, E.: Improving root separation bounds. Journal of Symbolic Computation **84** 25–56 (2018)

[43] Connelly, R., Fowler, P.W., Guest, S.D., Schulze, B., Whiteley, W.J.: When is a symmetric pin-jointed framework isostatic? International Journal of Solids and Structures **46**(3–4) 762–773 (2009)

[44] Guest, S.D., Fowler, P.W., Schulze, B.: Mobility of symmetric block-and-hole polyhedra. International Journal of Solids and Structures **150** 40–51 (2018)

[45] Möbius, A.F.: Der barycentrische Calcul. Verlag J.A. Barth (1827)

[46] Aichholzer, O., Jüttler, B.: Einführung in die angewandte Geometrie. Springer (2014)

[47] Nawratil, G.: Dataset: Snappability and singularity-distance of pin-jointed body-bar frameworks, Mendeley Data, V1, doi: 10.17632/n46vbrn93s.1 (2021)

[48] Pottmann, H., Wallner, J.: Computational Line Geometry. Springer (2001)

[49] Merlet, J.-P.: Singular Configurations of Parallel Manipulators and Grassmann Geometry. International Journal of Robotic Research **8**(5) 45–56 (1992)

[50] Nawratil, G.: Singularity Distance for Parallel Manipulators of Stewart Gough Type. Advances in Mechanism and Machine Science (T. Uhl ed.), pages 259–268, Springer (2019)

[51] Zein, M., Wenger, P., Chablat, D.: (2007) Singularity Surfaces and Maximal Singularity-Free Boxes in the Joint Space of Planar 3-RPR Parallel Manipulators. Proceedings of 12th IFToMM World Congress, Besançon, France, arXiv:0705.1409 (2007)

[52] Kapilavai, A., Nawratil, G.: Comparison of extrinsic and intrinsic singularity distance measures for planar 3-RPR manipulators. in preparation

[53] Kapilavai, A., Nawratil, G.: On homotopy continuation based singularity distance computations for 3-RPR manipulators. New Trends in Mechanism Science (D. Pisla, B. Corves eds.), pages 56–64, Springer (2020)

[54] Borras, J., Thomas, F., Torras, C.: New Geometric Approaches to the Analysis and Design of Stewart-Gough Platforms. IEEE/ASME Transactions on Mechatronics **19**(2) 445–455 (2014)

[55] Kresling, B.: Natural twist buckling in shells: from the Hawkmoth's bellows to the deployable Kresling-pattern and cylindrical Miura-ori. Proceedings of the 6th International Conference on Computation of Shell and Spatial Structures (J.F. Abel, J.R. Cooke eds.), Ithaca, NY (2008)

[56] Cai, J., Deng, X., Zhou, Y., Feng, J., Tu, Y.: Bistable behavior of the cylindrical origami structure with Kresling pattern. Journal of Mechanical Design **137** 061406 (2015)

[57] Guest, S.D., Pellegrino, S.: The folding of triangulated cylinders, Part I: Geometric considerations. Journal of Applied Mechanics **61**(4) 773–777 (1994)

[58] Guest, S.D., Pellegrino, S.: The folding of triangulated cylinders, Part III: Experiments. Journal of Applied Mechanics **63**(1) 77–83 (1996)

[59] Wittenburg, J.: Foldable and Self-Intersecting Polyhedral Cylinders Based on Triangles. Journal for Geometry and Graphics **23**(2) 245–258 (2019)

[60] Holmes-Cerfon, M.: Private communication (2020)

A   Examples of snapping model flexors

Within this appendix we discuss the examples of the Siamese dipyramid and the four-horn in detail and compare the obtained results with existing ones reported in the literature.

A.1   Siamese dipyramid

The original Siamese dipyramid (SD) introduced by Goldberg [23, page 167] consists of 20 equilateral triangles with an edge lengths of 1, which are arranged in two dipyramids with a hexagonal equatorial polygon (see Fig. 9, left). Note that we assume that the SD has a reflexion-symmetry with respect to two orthogonal planes. We can insert a coordinate frame in such a way that these planes are the xy-plane and the yz-plane, respectively.
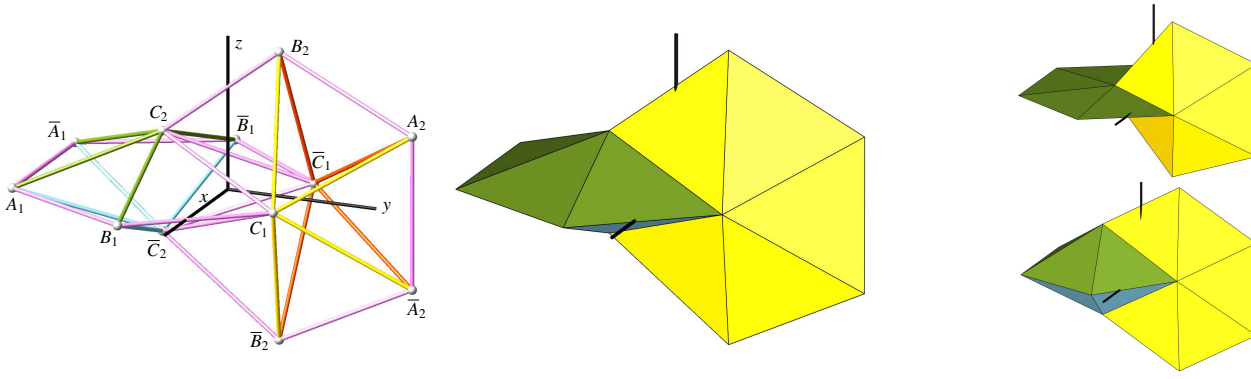
Fig. 9. Left: Illustration of the realization $G(\mathbf{V}_1)$ as a bar-joint framework together with the coordinate frame, where the axes are of length one. Center: The same configuration as on the left side but illustrated with panels instead of bars. Right: At the top the second realization $G(\mathbf{V}_2)$ is visualized and at the bottom the third one $G(\mathbf{V}_3)$.
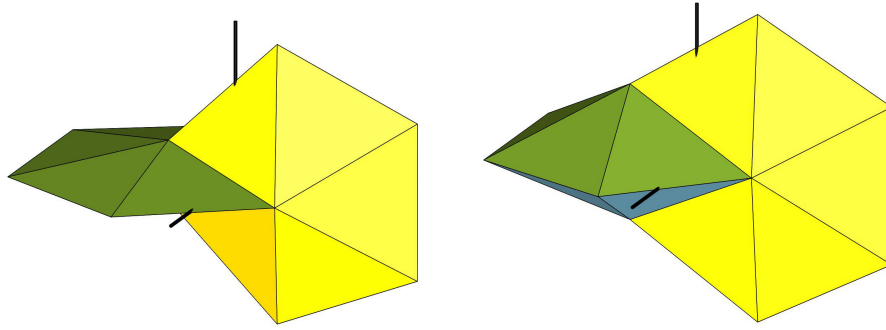

Fig. 10. On the left (resp. right) side the shaky saddle realizations $G(\mathbf{V}')$ (resp. $G(\mathbf{V}'')$) is illustrated, which is passed during the snap between $G(\mathbf{V}_1)$ and $G(\mathbf{V}_2)$ (resp. $G(\mathbf{V}_3)$). An animation of the snapping behavior can be downloaded from [47].

Then the vertices, which are noted according to Fig. 9, can be coordinatized as follows:

$$A_1 = (x_1, y_1, 0)^T \qquad \overline{A}_1 = (-x_1, y_1, 0)^T \qquad A_2 = (0, u_1, v_1)^T \qquad \overline{A}_2 = (0, u_1, -v_1)^T \qquad (49)$$

$$B_1 = (x_2, y_2, 0)^T \qquad \overline{B}_1 = (-x_2, y_2, 0)^T \qquad B_2 = (0, u_2, v_2)^T \qquad \overline{B}_2 = (0, u_2, -v_2)^T \qquad (50)$$

$$C_1 = (x_3, y_3, 0)^T \qquad \overline{C}_1 = (-x_3, y_3, 0)^T \qquad C_2 = (0, u_3, v_3)^T \qquad \overline{C}_2 = (0, u_3, -v_3)^T \qquad (51)$$

In addition we can assume without loss of generality that $u_3 = -y_3$ holds; i.e. the vertices C_1 and $\overline{C}_1$ have the same distance from the xz-plane as the points C_2 and $\overline{C}_2$. Therefore the total number of unknowns is 11.

It is well-known [23, 26] that the SD can snap out of the symmetric[17] realization $G(\mathbf{V}_1)$ (cf. Fig. 9, left/center) into one of the two asymmetric realizations $G(\mathbf{V}_2)$ and $G(\mathbf{V}_3)$, respectively (cf. Fig. 9, right). A simple procedure for the computation of these three undeformed realizations is given in [26]. We only give the numerical values of these configurations in Table 6.

A.1.1 Isostaticity and shakiness

The bar-joint framework of the SD is isostatic, because every closed polyhedral surface of genus 0 with triangular faces has this property[18]. This isostaticity remains intact under the assumption of the 2-fold reflexion-symmetry, as it only corresponds to the identification of some of the coordinates within the structure.

The SD is in a shaky configuration if the rank of its rigidity matrix $\mathbf{R}_{G(\mathbf{V})}$ is less than 30. From this one can compute the algebraic characterization, which corresponds to the vanishing of the following polynomial

---

[17]With respect to the height of the two dipyramids.

[18]This can easily be followed from Euler's polyhedral formula.

	$\mathbf{V}_1$	$\mathbf{V}_2$	$\mathbf{V}'$ (bar-joint)	$\mathbf{V}'$ (panel-hinge)
x_1	-0.5	-0.5	-0.501499108259	-0.501518680610
x_2	-0.940024410925	-0.997453425271	-0.979262620688	-0.979200605399
x_3	-0.327267375345	-0.492373245899	-0.432379113707	-0.432385909548
y_1	-1.245032582350	-1.296828963170	-1.282364611843	-1.282380966624
y_2	-0.347046770776	-0.429338277522	-0.400464708308	-0.400381868195
y_3	0.443224584739	0.433734148410	0.440320490435	0.440337472811
u_1	1.245032582350	1.146172627664	1.193026874842	1.192998833484
u_2	0.347046770776	0.205744933405	0.273852988315	0.273969061570
v_1	0.5	0.5	0.498976790866	0.498943974578
v_2	0.940024410925	0.839993752693	0.887603513697	0.887698700553
v_3	0.327267375345	0.071185256433	0.190566289070	0.190551925851

Table 6. Coordinates of the undeformed realizations $G(\mathbf{V}_1)$ and $G(\mathbf{V}_2)$, respectively, and of the shaky saddle realization $G(\mathbf{V}')$ with respect to the two different interpretations. The coordinates of $G(\mathbf{V}_3)$ and $G(\mathbf{V}'')$ can be obtained from $G(\mathbf{V}_2)$ and $G(\mathbf{V}')$ by the following exchange of coordinate entries: $x_i \leftrightarrow -v_i$ and $y_i \leftrightarrow -u_i$ for $i = 1, 2, 3$.

$$\underbrace{v_3(x_1y_2 + x_1y_3 - x_2y_1 - x_2y_3)}_{\mathrm{copl}(C_2,\overline{C}_2,A_1,B_1)}\underbrace{v_3(2x_2y_3 - x_3y_2 - x_3y_3)}_{\mathrm{copl}(C_2,\overline{C}_2,B_1,C_1)}\underbrace{x_3(u_1v_2 - u_2v_1 + v_1y_3 - v_2y_3)}_{\mathrm{copl}(C_1,\overline{C}_1,A_2,B_2)}\underbrace{x_3(u_2v_3 + 2v_2y_3 - v_3y_3)}_{\mathrm{copl}(C_1,\overline{C}_1,B_2,C_2)}S \qquad (52)$$

where copl indicates the coplanarity of the vertices given in the round bracket. For the condition $x_3 = 0$ or $v_3 = 0$ one of the two dipyramids is even in a flat configuration. Beside these geometric simple cases of shakiness we also have the factor[19] S, which denotes an algebraic expression with 374 terms and a total degree of 9. Interestingly S is only quadratic with respect to the two non-zero coordinates of the following points: $A_i, B_i, \overline{A}_i$ and $\overline{B}_i$ for $i = 1, 2$. For the points A_i and $\overline{A}_i$ it is even linear in x_1 (for $i = 1$) or v_1 (for $i = 2$).

Moreover, if the infinitesimal flexibility of the SD interpreted as bar-joint framework does not result from the degeneration of a triangular substructure into a collinear arrangement, then the corresponding panel-hinge framework is also shaky.

A.1.2 Interpretation as a bar-joint structure

We set up our formulation of the deformation energy density u under the assumption that the SD keeps the 2-fold reflexion-symmetry during the deformation. The obtained system of 11 equations ∇u results in 177 147 paths within a total degree homotopy (cf. [40]). The path tracking done by the software Bertini ends up in 22 153 finite real solutions (set $\mathscr{R}$). After reduction to the set $\mathscr{S}$ we remain with 21 904 solutions. This set is the input for the algorithm described in Section 4.2, which outputs the two shaky saddle realizations $G(\mathbf{V}')$ and $G(\mathbf{V}'')$, respectively, displayed in Fig. 10. The numerical values of these realizations are also given in Table 6.

We get $s(\mathbf{L}) = s(\mathbf{V}_1) = s(\mathbf{V}_2) = s(\mathbf{V}_3) = 1.661376004928 \cdot 10^{-6}$ and due to Theorem 5 (under consideration of Corollary 1) this value also equals $\varsigma(\mathbf{L}) = \varsigma(\mathbf{V}_1) = \varsigma(\mathbf{V}_2) = \varsigma(\mathbf{V}_3)$.

Comparison with the results obtained in [27]: According to [27] there exists a realization within the deformation path between two snapping realizations $G(\mathbf{V}_1)$ and $G(\mathbf{V}_{2/3})$, where the value for $e := \sqrt{\sum_{ij}(L_{ij}^2 - L_{ij}'^2)^2}$ is greater or equal to a value e_{min}^* given by $2.98 \cdot 10^{-4}$ for $G(\mathbf{V}_1)$ and $3.35 \cdot 10^{-4}$ for $G(\mathbf{V}_{2/3})$, respectively. As noted in [27] the value e_{min}^* is a minimum bound and does not say how close this bound is to the true barrier.

By our approach we can determine this true barrier value numerically as $e_{min} = 1.996823079751 \cdot 10^{-2}$, which has to be the same for the three realizations $G(\mathbf{V}_i)$ for $i = 1, 2, 3$ due to the snapping between these realizations. Therefore the true barrier is approximately 67 times and 60 times, respectively, larger then the given e_{min}^* value.

From e_{min}^* one can also approximate the length $\Delta L_{\varnothing}^*$, which an edge must change in average according to [27, Example 2], yielding the values $2.720355368942 \cdot 10^{-5}$ and $3.058117612737 \cdot 10^{-5}$, respectively. Based on $G(\mathbf{V}')$ we can also compute the absolute average change $\Delta L_{\varnothing}^{abs} = 1.673630072024 \cdot 10^{-3}$ (which equals also the relative average change $\Delta L_{\varnothing}^{rel}$ as the

---

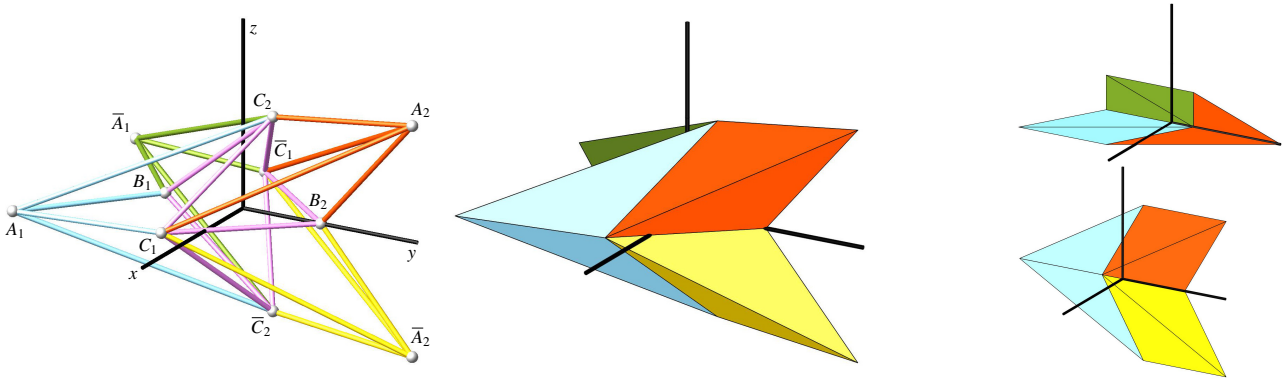[19]It can be downloaded from [47].

Fig. 11. Left: Illustration of the realization $G(\mathbf{V}_1)$ of the original four-horn as a bar-joint framework together with the coordinate frame, where the axes are of length one. Center: The same configuration as on the left side but illustrated with panels instead of bars. Right: The two flat realizations are visualized, where $G(\mathbf{V}_2)$ is displayed at the top and $G(\mathbf{V}_3)$ at the bottom.
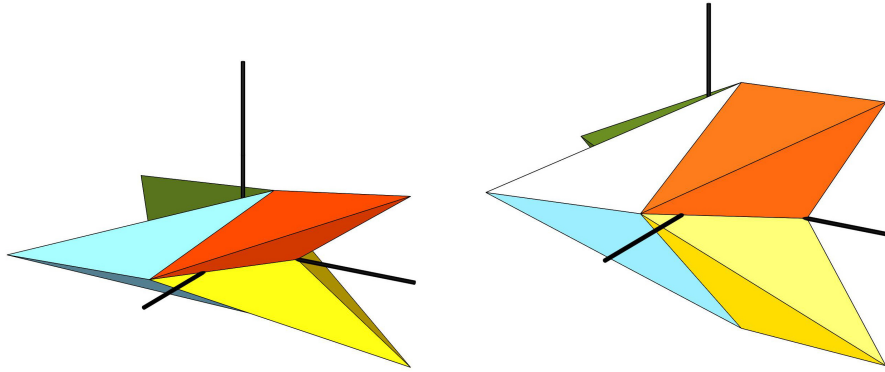

Fig. 12. On the left (resp. right) side the shaky saddle realizations $G(\mathbf{V}')$ (resp. $G(\mathbf{V}'')$) of the design FH_1 is illustrated, which is passed during the snap between $G(\mathbf{V}_1)$ and $G(\mathbf{V}_2)$ (resp. $G(\mathbf{V}_3)$). An animation of the snapping behavior can be downloaded from [47].

initial length of the edges is 1). Therefore it is 62 times and 55 times, respectively, larger than the values resulting from the data given in [27].

Comparison with the results obtained in [26]: The intrinsic index given in [26] equals $\Delta L^*_{max} = 3.94 \cdot 10^{-3}$ and correspond to the maximal relative (with respect to the initial length of 1) change in the length of an edge during the deformation. But it should be noted that the setup of the pyramids in [26] is more restrictive than ours, as all edges through the vertices C_1, $\overline{C}_1$ and C_2, $\overline{C}_2$ cannot be deformed and have a fixed length of 1; all other edges are restricted to have the same length.

Based on $G(\mathbf{V}')$ we can also compute this maximal relative change ΔL^{rel}_{max} of an edge as $2.998216519082 \cdot 10^{-3}$ (which equals also the maximal absolute change ΔL^{abs}_{max} as the initial length of the edges is 1). Therefore the value reported in [26] is 31% larger than ours.

Remark 13. *In [26] and [27] also some indices are given to estimate/quantify the variations of the spatial shape of the snapping framework. Due to their extrinsic nature they cannot give information about the snappability, which only depends on the intrinsic geometry.* ⋄

A.1.3 Interpretation as a panel-hinge structure

The same study can also be done by considering the SD as a polyhedral surface composed of triangular panels with a Poisson ratio of $v = 1/2$. The tracking of the 177 147 paths of a total degree homotopy using Bertini ends up in 20305 real solutions, which can be reduced to 20056 solutions of the set $\mathscr{S}$. In this case we get $s(\mathbf{L}) = s(\mathbf{V}_i) = \varsigma(\mathbf{V}_i) = \varsigma(\mathbf{L}) = 4.466362657431 \cdot 10^{-6}$ for $i = 1, 2, 3$.

A.2 Four-horn

The original four-horn (FH) was introduced by Casper Schwabe at the *Phänomena* exposition 1984 in Zürich, Switzerland (cf. Fig. 11). From the combinatorial point of view the FH equals a SD with pentagonal equatorial polygons. In contrast to a SD, a FH does not consist of congruent equilateral face-triangles but of congruent isosceles ones where α denotes the angle enclosed by the base of length $b > 0$ and the leg of length $a > 0$. Under consideration of the two-fold reflexion-symmetry with respect to two orthogonal planes, we can insert a Cartesian frame in such a way, that the vertices, which are noted according to Fig. 11, are coordinatized as follows:

$$A_1 = (x_1, y_1, 0)^T \qquad \overline{A}_1 = (-x_1, y_1, 0)^T \qquad B_1 = (0, y_2, 0)^T \qquad C_1 = (x_3, y_3, 0)^T \qquad \overline{C}_1 = (-x_3, y_3, 0)^T \qquad (53)$$

$$A_2 = (0, u_1, v_1)^T \qquad \overline{A}_2 = (0, u_1, -v_1)^T \qquad B_2 = (0, u_2, 0)^T \qquad C_2 = (0, u_3, v_3)^T \qquad \overline{C}_2 = (0, u_3, -v_3)^T \qquad (54)$$

As in Appendix A.1 we can assume without loss of generality that $u_3 = -y_3$ holds.

It is well-known that the FH can snap out of the symmetric realization $G(\mathbf{V}_1)$ into one of the two flat realizations $G(\mathbf{V}_2)$ and $G(\mathbf{V}_3)$, respectively, which are both shaky due to their planarity. According to [25] these three undeformed realizations, which are displayed in Fig. 11, exist for all choices of a and b with $2a > b$.

As done in [25] we will distinguish three different designs FH_i $i = 1, 2, 3$ of four-horns, which differ in the lengths of the leg a_i and base b_i with

$$a_1 = 3\sqrt{2} + 6 - \frac{3}{2}\sqrt{20 + 14\sqrt{2}} \qquad a_2 = 6 - 3\sqrt{3} \qquad a_3 = 6\sqrt{3} + 12 - \frac{(9\sqrt{3} + 15)\sqrt{2}}{2} \qquad (55)$$

$$b_1 = 3\sqrt{20 + 14\sqrt{2}} - 6\sqrt{2} - 9 \qquad b_2 = 6\sqrt{3} - 9 \qquad b_3 = (9\sqrt{3} + 15)\sqrt{2} - 12\sqrt{3} - 21 \qquad (56)$$

For these values, which result in an average edge length of 1, we get the angles $\alpha_1 = 22.5°$ (the original design of Schwabe), $\alpha_2 = 30°$ and $\alpha_3 = 15°$, respectively.

How the coordinates of the vertices can be computed for the two flat realizations $G(\mathbf{V}_2)$ and $G(\mathbf{V}_3)$ and the symmetric realization $G(\mathbf{V}_1)$ of these three designs FH_i can be looked up in [25]. We only give the numerical values of these realizations in the Tables 9–11.

A.2.1 Isostaticity and shakiness

The FH is isostatic for the same reasons as pointed out in A.1.1. Moreover, we can also determine the algebraic condition of shakiness in an analogous way, which yields:

$$x_1 x_3^2 v_1 v_3^2 \underbrace{v_3(2x_1 y_3 - x_3 y_1 - x_3 y_3)}_{copl(C_2, \overline{C}_2, A_1, C_1)} \underbrace{x_3(u_1 v_3 + 2v_1 y_3 - v_3 y_3)}_{copl(C_1, \overline{C}_1, A_2, C_2)} S = 0 \qquad (57)$$

where $x_1 = 0$ means that the triangles (A_1, B_1, C_2) and $(A_1, B_1, \overline{C}_2)$ coincide with $(\overline{A}_1, B_1, C_2)$ and $(\overline{A}_1, B_1, \overline{C}_2)$, respectively. The same holds for the condition $v_1 = 0$ by swapping the indices 1 and 2 for the above given triangles. For the condition $x_3 = 0$ or $v_3 = 0$ two out of the four horns are in a flat configuration. Beside these geometric simple cases of shakiness we also have the factor[20] S, which denotes an algebraic expression with 110 terms and a total degree of 9. Again S is only quadratic with respect to the two non-zero coordinates of A_i and $\overline{A}_i$, respectively, for $i = 1, 2$.

A.2.2 Interpretation as a bar-joint structure

For the three designs FH_i for $i = 1, 2, 3$ we compute similar to the SD example given in Appendix A.1 the shaky saddle realizations $G(\mathbf{V}')$ and $G(\mathbf{V}'')$, respectively, which are displayed in Fig. 12 for FH_1. The numerical values of these realizations are also given in the Tables 9–11. For all three designs the relation $s(\mathbf{L}) = s(\mathbf{V}_i) = \varsigma(\mathbf{V}_1)$ holds true for $i = 1, 2, 3$ (due to Theorem 5 under consideration of Corollary 1) as well as $\varsigma(\mathbf{L}) = \varsigma(\mathbf{V}_2) = \varsigma(\mathbf{V}_3) = 0$. Moreover, we calculated for all three designs FH_i the additional values e_{min}, $\Delta L_{\varnothing}^{abs}$, $\Delta L_{\varnothing}^{rel}$, ΔL_{max}^{abs} and ΔL_{max}^{rel} as in the case of the SD. For a better comparison they are arranged in the Tables 7 and 8, respectively.

Comparison with the method presented in [27]: According to [60] the minimum bound e_{min}^* of FH_1's realization $G(\mathbf{V}_1)$ equals $4.0458 \cdot 10^{-4}$, which is approximately 1/6 of the true barrier e_{min} (cf. Table 7). Moreover, e_{min}^* implies an approximation of the absolute length $\Delta L_{\varnothing}^* = 4.129227333 \cdot 10^{-5}$ an edge must change in average, which is about 23% of the value $\Delta L_{\varnothing}^{abs}$ (cf. Table 7).

---

[20]It can be downloaded from [47].

	# tracked paths	#$\mathscr{R}$	#$\mathscr{S}$	$s(\mathbf{L}) = \varsigma(\mathbf{V}_1)$	e_{min}
FH$_1$	19 683	924	863	$1.753810068479 \cdot 10^{-8}$	$2.503636587824 \cdot 10^{-3}$
FH$_2$	19 683	917	819	$2.035395987407 \cdot 10^{-7}$	$1.663070753397 \cdot 10^{-2}$
FH$_3$	19 683	923	897	$9.864008781699 \cdot 10^{-11}$	$1.944647875494 \cdot 10^{-4}$

Table 7. Computational data for the three designs FH$_1$, FH$_2$ and FH$_3$. Note that the computation of the set $\mathscr{R}$ was done by a total degree homotopy using Bertini.

	$\Delta L_{\varnothing}^{abs}$	$\Delta L_{\varnothing}^{rel}$	ΔL_{max}^{abs}	ΔL_{max}^{rel}
FH$_1$	$1.755195468044 \cdot 10^{-4}$	$1.684100667119 \cdot 10^{-4}$	$2.932163649725 \cdot 10^{-4}$	$2.318551827789 \cdot 10^{-4}$
FH$_2$	$1.219270735675 \cdot 10^{-3}$	$1.174975973629 \cdot 10^{-3}$	$2.061810888944 \cdot 10^{-3}$	$1.830418324804 \cdot 10^{-3}$
FH$_3$	$1.315683847557 \cdot 10^{-5}$	$1.257398895852 \cdot 10^{-5}$	$2.221096435873 \cdot 10^{-5}$	$1.598717509714 \cdot 10^{-5}$

Table 8. Continuation of Table 7.

Remark 14. *For the flat realizations the method of [27] does not work, as they are not pre-stressed stable. Therefore we cannot compare the method of [27] with the values obtained by our method regarding $G(\mathbf{V}_2)$ and $G(\mathbf{V}_3)$, respectively.* ◇

Comparison with the results obtained in [25]: The authors of [25] sliced the four-horn along the polylines $C_1C_2\overline{C}_1$ and $C_1\overline{C}_2C_1$ with exception of the points C_1 and $\overline{C}_1$. In this way they get two two-horns, which are linked over the points C_1 and $\overline{C}_1$. Maintaining the 2-fold reflexion-symmetry, the resulting structure has a one-parametric mobility. Apart from the configurations $G(\mathbf{V}_1)$, $G(\mathbf{V}_2)$ and $G(\mathbf{V}_3)$ the points on both two-horns, which correspond to the point C_2 do not coincide. This mismatch of points is measured by the relative error in the z-coordinate. The maximum of this relative error during the flexion of the two two-horns between the two flat configurations equals the index given in [25]. Therefore this index is also of extrinsic nature, but the authors of [25] also noted an empirical rule of thumb without further explanation, which reads as $\delta^* = 0.018 \cdot (\alpha/10)^4\%$ where α has to be inserted in degree. This formula only depends on the intrinsic geometry of the framework.

For our considered values α_i for $i = 1,2,3$ we get $\delta_1^* = 0.4613203125\%$, $\delta_2^* = 1.458\%$ and $\delta_3^* = 0.091125\%$. As this index δ^* cannot be compared one-to-one with any of our given values, we can evaluate the index δ^* by considering the relation $\delta_1^* : \delta_2^* : \delta_3^*$. It can easily be seen that this relation does not go along with the corresponding relation of any of the values $s(\mathbf{L})$, e_{min}, $\Delta L_{\varnothing}^{abs}$, $\Delta L_{\varnothing}^{rel}$, ΔL_{max}^{abs} and ΔL_{max}^{rel}, respectively, given in Tables 7 and 8.

A.2.3 Interpretation as a panel-hinge structure

The same study can also be done by considering the FH as a polyhedral surface composed of triangular plates with a Poisson ratio of $\nu = 1/2$. We track for each of the three designs 19 683 paths of a total degree homotopy performed with Bertini. The computations end up in 1 259 real solutions for FH$_1$ (1 457 for FH$_2$ and 1 324 for FH$_3$). After reduction to the set $\mathscr{S}$ we remain with 1 242 realizations for FH$_1$ (1 360 for FH$_2$ and 1 238 for FH$_3$). Also for the interpretation as a panel-hinge structure the relations $\varsigma(\mathbf{L}) = \varsigma(\mathbf{V}_2) = \varsigma(\mathbf{V}_3) = 0$ and $s(\mathbf{L}) = s(\mathbf{V}_i) = \varsigma(\mathbf{V}_1)$ ($i = 1,2,3$) hold true for all three designs. The corresponding value equals $1.748173013469 \cdot 10^{-6}$ for FH$_1$ ($2.340885199965 \cdot 10^{-5}$ for FH$_2$ and $6.288380657092 \cdot 10^{-8}$ for FH$_3$).

	$\mathbf{V}_1$	$\mathbf{V}_2$	$\mathbf{V}'$ (bar-joint)	$\mathbf{V}'$ (panel-hinge)
x_1	-0.439833121345	-0.551313194956	-0.514676938265	-0.513910947926
x_3	-0.402578359944	-0.551313194956	-0.496123528337	-0.495616858966
y_1	-1.045126760122	-1.055331194900	-1.049041632768	-1.047987400977
y_2	-0.401357155967	-0.504017999944	-0.463165051665	-0.461829297096
y_3	-0.266342733180	-0.275656597478	-0.269426558812	-0.269389463808
u_1	1.045126760122	1.055331194900	1.047880696191	1.048797729978
u_2	0.401357155968	0.275656597478	0.331798913977	0.332716034007
v_1	0.439833121346	0	0.308030377883	0.310260240907
v_3	0.402578359945	0	0.267213277407	0.268392688481

Table 9.   Coordinates of the undeformed realizations $G(\mathbf{V}_1)$ and $G(\mathbf{V}_2)$ of the design FH$_1$ and of the shaky saddle realization $G(\mathbf{V}')$ of FH$_1$ with respect to the two different interpretations. The coordinates of $G(\mathbf{V}_3)$ and $G(\mathbf{V}'')$ can be obtained from $G(\mathbf{V}_2)$ and $G(\mathbf{V}')$ by the following exchange of coordinate entries: $x_j \leftrightarrow -v_j$ for $j = 1, 3$ and $y_i \leftrightarrow -u_i$ for $i = 1, 2, 3$.

	$\mathbf{V}_1$	$\mathbf{V}_2$	$\mathbf{V}'$ (bar-joint)	$\mathbf{V}'$ (panel-hinge)
x_1	-0.610560396069	-0.696152422706	-0.674892191647	-0.673709307095
x_3	-0.514152040259	-0.696152422706	-0.629718504095	-0.630052932256
y_1	-0.969412109993	-1.004809471616	-0.984812341395	-0.981100971148
y_2	-0.446547949553	-0.602885682969	-0.546021679456	-0.541654138725
y_3	-0.171366775159	-0.200961894323	-0.181083746571	-0.180980608226
u_1	0.969412109993	1.004809471616	0.975854359558	0.978589555099
u_2	0.446547949553	0.200961894323	0.316170888257	0.318169735899
v_1	0.610560396069	0	0.457391731880	0.463293753345
v_3	0.514152040259	0	0.344387159440	0.344641218655

Table 10.   The analogous table to Table 9 but with respect to the design FH$_2$.

	$\mathbf{V}_1$	$\mathbf{V}_2$	$\mathbf{V}'$ (bar-joint)	$\mathbf{V}'$ (panel-hinge)
x_1	-0.284308975844	-0.381499642545	-0.346332965123	-0.345941194845
x_3	-0.274123668705	-0.381499642545	-0.341068732408	-0.340681988409
y_1	-1.091519316228	-1.093387667069	-1.092180085853	-1.092027657175
y_2	-0.383468247941	-0.432610903111	-0.412298335661	-0.412002561558
y_3	-0.328588016197	-0.330388381978	-0.329187289575	-0.329179948495
u_1	1.091519316228	1.093387667069	1.092099843041	1.092235340815
u_2	0.383468247944	0.330388381978	0.353323819879	0.353582747289
v_1	0.284308975853	0	0.190684818526	0.191590754090
v_3	0.274123668714	0	0.179953619106	0.180744480102

Table 11.   The analogous table to Table 9 but with respect to the design FH$_3$.